Kaunas University of Technology

Faculty of Mathematics and Natural Sciences

Developing of white hybrid organic light-emitting devices by solution-processing utilizing novel iridium (III) complexes

Master's Final Degree Project

Karolis Leitonas

Project author

Dr. Dmytro Volyniuk

Supervisor

Kaunas, 2020

Kaunas University of Technology

Faculty of Mathematics and Natural Sciences

Developing of white hybrid organic light-emitting devices by solution-processing utilizing novel iridium (III) complexes

Master's Final Degree

Materials Science (6211FX009)

Karolis Leitonas

Project author

Dr. Dmytro Volyniuk

Supervisor

Lect. Dr. Darius Virbukas

Reviewer

Kaunas, 2020

Kaunas University of Technology

Faculty of Mathematics and Natural Sciences

Karolis Leitonas

Developing of white hybrid organic light-emitting devices by solution-processing utilizing novel iridium (III) complexes

Declaration of Academic Integrity

I confirm that the final project of mine, Karolis Leitonas, on the topic „Developing of white hybrid organic light-emitting devices by solution-processing utilizing novel iridium (III) complexes“ is written completely by myself; all the provided data and research results are correct and have been obtained honestly. None of the parts of this thesis have been plagiarised from any printed, Internet-based or otherwise recorded sources. All direct and indirect quotations from external resources are indicated in the list of references. No monetary funds (unless required by Law) have been paid to anyone for any contribution to this project.

I fully and completely understand that any discovery of any manifestations/case/facts of dishonesty inevitably results in me incurring a penalty according to the procedure(s) effective at Kaunas University of Technology.

(name and surname filled in by hand)

(signature)

Leitonas, Karolis. Developing of white hybrid organic light-emitting devices by solution-processing utilizing novel iridium (III) complexes. Master's Final Degree Project / supervisor Dr. Dmytro Volyniuk; Faculty of Mathematics and Natural Sciences, Kaunas University of Technology.

Study field and area (study field group): Technological Sciences, Materials Technologies (F03).

Keywords: white, organic, semiconductor, OLED.

Kaunas, 2020. 58 pages.

Summary

Increasing demand of organic light emitting diodes (OLED) in lighting and display markets are associated with excellent electroluminescence (EL) spectra quality (absent emission in UV/infrared spectral region, smooth EL spectra without sharp spikes, high colour purity, etc.) and flexibility/optical transparency of commercial products offered by this technology. Due to huge interest of consumers, many scientists are working on further improvements of electricity-light conversion efficiency, operation stability, EL spectra quality of OLEDs. Therefore, input of this study is aimed towards fabricating human eyes friendly white colour OLEDs with excellent electroluminescent properties, which is one of the top priorities in the OLED community.

In this work, white hybrid OLEDs were developed using two newly synthesized iridium (III) complexes with phosphorescence emission in orange or deep-red colour regions. Before OLED development, the chosen complexes were precisely investigated by photophysical, electrochemical and photoelectrical techniques in order to verify the potential of them to be used as a phosphorescent emitters in optoelectronic applications. The analysed compounds exhibited photoluminescence (PL) emission in orange and deep red regions with PL decays in microseconds range and PL quantum yield extending up to 60%. The solid-state layers based on the investigated molecules were characterized by ionization potentials falling in range of 5.17–5.4 eV and identical electron affinity value of 2.87eV. In the proposed device structure of white OLEDs, blue fluorescent, green thermally activated delayed fluorescent (TADF), and phosphorescent emitter were mixed in the light-emitting layer for obtaining white electroluminescence. For OLED fabrication, phosphorescent (triplet) and TADF emitters were selected due to their light-emissive singlet and triplet exciton recombination probability (theoretically 100%). In device structures, the blue fluorescent emitter additionally acted as the host for green and red emitters in the light-emitting layer. Ultralow concentrations of these emitters were optimized for preventing full energy transfer from the host to green TADF and red phosphorescent emitters. In case of usage of deep-red phosphorescent emitter, high-quality white electroluminescence with colour rendering index reaching 85 was observed from the hybrid, partially solution-processed, OLEDs exhibiting maximum brightness exceeding 10000 cd/m^2 and high external quantum efficiency of 6.3%. In case of using orange phosphorescent emitter, white hybrid devices were characterized by high quality (human-eyes-friendly) electroluminescence with CIE1931 coordinates of (0.34, 0.39), colour temperature of 2910 K and colour rendering index of 72 as well as high maximum external quantum efficiency of 8.7%.

Leitonas, Karolis. Baltai šviečiančių, hibridinių organinių šviesos diodų formuojamų tirpalų liejimo būdu tobulinimas, panaudojant naujus iridžio (III) kompleksus. Magistro studijų baigiamasis projektas / vadovas Dr. Dmytro Volyniuk; Kauno technologijos universitetas, Matematikos ir gamtos mokslų fakultetas.

Studijų kryptis ir sritis (studijų krypčių grupė): Technologijų mokslai; Medžiagų technologijos (F03).

Reikšminiai žodžiai: organinis, puslaidininkis, baltas, OLED.

Kaunas, 2020. 58 p.

Santrauka

Kylantis organinių šviesos diodų (OLED) poreikis apšvietimo ir ekranų rinkose yra siejamas su puikiomis raiškos savybėmis (tolygi emisija regimajame diapazone, aukštas spalvų grynumas ir t. t.) ir ypatingai lanksčiomis šios technologijos pritaikymo galimybėmis. Dėl didelio vartotojų susidomėjimo, daugybė mokslininkų stengiasi ir toliau pagerinti OLED savybes tokias kaip efektyvesnė elektros-šviesos konversija, geresnis spalvų atkūrimas, ryškumas, ilgaamžiškumas ar tiesiog kaina. Atsižvelgiant į tai, šio darbo tikslas yra sukurti OLED prietaisus, kurie pasižymėtų žmogaus akių nedirginančia spalva su puikiomis elektroliuminescencijos savybėmis.

Šiame darbe, panaudojus du naujai susintetintus iridžio (III) kompleksus su emisija oranžiniame ir raudoname spalvų regionuose, buvo pagaminti baltai šviečiantys hibridiniai OLED. Pirmiausia, siekiant patikrinti galimybę iridžio (III) kompleksus panaudoti optoelektroniniuose prietaisuose kaip fosforescencinius spinduolius, buvo panaudoti optiniai, eleketrocheminiai ir fotoelektriniai tyrimų metodai. Medžiagos pasižymėjo fotoliuminescencija oranžinės ir raudonos spalvų regionuose, emisijos gesimo trukmės buvo mikrosekundžių intervale, o fotoliuminescencijos kvantinės išeigos siekė iki 60 %. Tirtų medžiagų kietų sluoksnių jonizacijos energijos buvo išmatuotos 5.17–5.4 eV intervale, o elektronų gimiringumas buvo vienodas – 2.87 eV. Siekiant išgauti baltos spalvos elektroliuminescenciją, buvo nuspręsta naudoti hibridinį, liejimo iš tirpalų būdu pagamintą, emisinį šviestuko sluoksnį – sumaišyti fluorescencinę mėlyną, šiluma aktyvuotos uždelstos fluorescencijos (angl. *thermally activated delayed fluorescence,* TADF) žalią ir fosforescencinę raudoną spalvas. Keičiant santykį tarp spalvų komponenčių emisiniame sluoksnyje, pavyko išgauti puikias elektroliuminescencines prietaisų savybes. Baltos spalvos OLED su panaudotu raudonos spalvos iridžio (III) kompleksu pasižymėjo aukštu spalvų atgavos rodikliu (angl. *colour rendering index,* CRI), kuris siekė 85. Išmatuotas skaistis viršijo 10000 cd/m^2, o išorinis kvantinis našumas – 6.3 %. Panaudojus oranžinės spalvos fosforescencinį spinduolį buvo gauta šilto atspalvio balta elektroliuminescencija, kuri yra artima natūraliai gamtos baltai spalvai. Prietaisai buvo charakterizuoti Tarptautinės apšvietimo komisijos (pranc. *Commission Internationale de l'Eclairage,* CIE) spalvų erdvės koordinatėmis (0,34; 0,39), susietąja spalvine temperatūra (angl. *correlated colour temperature,* CCT) – 2910 K, spalvų atgavos rodikliu – 72 ir aukštu išoriniu kvantiniu našumu – 8.7 %.

Table of contents

List of figures

List of tables

List of abbreviations

CCT – correlated colour temperature

CE – current efficacy

CIE – fr. *Commission internationale de l'éclairage* (eng. International commission of illumination)

CRI – colour rendering index

CT – charge transfer

CV – cyclic voltammetry

DAcIPN – 4,6-di(9,9-dimethylacridan-10-yl)isophthalonitrile

DACT-II – 9-[4-(4,6-diphenyl-1,3,5-triazin-2-yl)phenyl]-N,N,N′,N′-tetraphenyl-9H-carbazole3,6-diamine

DF – delayed fluorescence

EBL – electron blocking layer

EIL – electron injection layer

EL – electroluminescence

EML – emitting layer

EQE – external quantum efficiency

ETL – electron transporting layer

HBL – hole blocking layer

HIL – hole injection layer

HOMO -highest occupied molecular orbital

HTL – hole transporting layer

IC – internal conversion

IP – ionisation potential

IQE – internal quantum efficiency

ISC – intersystem crossing

ITO – indium tin oxide

LCD – liquid crystal display

LED – light emitting diode

LUMO – lowest unoccupied molecular orbital

mCP – 1,3-bis(9-carbazolyl)benzene

MO – molecular orbital

NPB – N,N′-Di(1-naphthyl)-N,N′-diphenyl-(1,1′-biphenyl)-4,4′-diamine

NTSC – National Television System Committee

OFET – organic field-effect transistor

OLED – organic light emitting diode

OSC – organic solar cell

PE – power efficacy

PLQY – photoluminescence quantum yield

RGB – red green blue

RISC – reverse intersystem crossing

TADF – thermally activated delayed fluorescence

TCTA – tris(4-carbazoyl-9-ylphenyl)amine

THF – tetrahydrofuran

TPBi – 2,2',2''-(1,3,5-Benzinetriyl)-tris(1-phenyl-1-H-benzimidazole)

TSPO1 – diphenyl-4-triphenylsilyl-phenylphosphineoxide

TTA – triplet-triplet annihilation

UV – ultraviolet

Introduction

Since invention of the lightbulb, artificial lighting became inevitable part of our daily routine. Nowadays man-made light can be observed everywhere you take your look on. In the house you have a number of lightbulbs illuminating your rooms, bright TVs or computers screens for entertainment or work purposes. Take a look in your own pocket and you will be welcomed by ultra-high definition display of smartphone. If you go outside – you see car headlights, street lighting, illuminated advertisements, etc. Even if you point your eyes to the sky – at night you can see blinking lights of airplanes or satellites.

In recent years, less efficient lighting solutions, such as incandescent, halogen, fluorescent, are being actively replaced by semiconductor-based, solid-state technology which is strongly dominating the market of lighting due to its superior efficiency and flexibility of application[1]. Mainly this technology can be divided in to two groups, according to the type of semiconductor used: one is based on inorganic semiconductors – light emitting diodes (LED) and the other is based on organic semiconductor technology – organic light emitting diodes (OLED)[2]. While LEDs, due to crystallinity of inorganic semiconductors, are considered as an excellent point light source, however OLEDs are opposite – it works best as a very thin, area emitting light sources, so it can be mounted directly on ceilings or walls as a planar sheet of light[3]. In fact, today OLED is a leading technology in display market, since it has many advantages compared to the other popular display alternatives such as liquid crystal display (LCD). OLED monitors are famous not only for the brilliant quality of displayed picture but for being "future-proof" as well, because OLEDs can be produced on flexible or even transparent substrates, which means that various wearable electronics with unprecedented form factor can be designed[3].

By default LEDs and OLEDs happened to have a trend of cold looking white colour with bluish tone and as a result of that, some biologic functions of humans have been negatively impacted[4]. Many studies have shown that blue light has the ability to control the body clock and stimulate alertness, memory and cognition. The key mechanism is that blue light stimulates the secretion of melatonin hormone in pineal gland and consequently can increase or decrease cortisol expression depending on time of day and regulate circadian rhythm of human[4, 5, 6, 7, 8]. Therefore, it is important to further research and develop devices with white colour which would have less negative impact for human health.

The aim of this work is to develop solution-processed white hybrid OLEDs with high quality electroluminescence featuring either high colour rendering index (CRI), close to nature white CIE1931 coordinates of (0.33, 0.33), or human eyes friendly colour temperature of near to 3000 K, by utilising newly synthesised iridium (III) complexes.

The tasks performed to achieve the aim:

1. investigate photophysical, electrochemical and photoelectrical properties of newly synthesised iridium (III) complexes;
2. design, fabricate and characterize prototype OLEDs using investigated emitters;
3. optimise device structures in order to get high quality white electroluminescence.

1. Literature review

1.1. Organic molecules

Organic molecules is a definition which describes a massive class of compounds, which all have mainly carbon-based structure and often contain other elements included, such as oxygen, hydrogen, sulphur, nitrogen and etc. Organic compounds can be classified in multiple ways, one of them is by origin: natural organic compounds are produced by living organisms (e.g. sugars, vitamins, hormones), synthetic organic compounds, as the name suggests, are artificially produced in laboratories (i.e. organic semiconductors or drugs). Other significant classification can be made according to the size of molecule. Small molecule organic materials are those with molecular weight lower than 1000 g/mol (e.g. carbazole) (Fig. 1). Polymers often have way larger molecular weight and have chain-like structure, which smallest repeated component is called a monomer. If the polymer is made from only one monomer – it is called a homopolymer (e.g. Poly(9-vinylcarbazole) (PVK)) (Fig. 1), if more than one monomer – it is called copolymer[9].

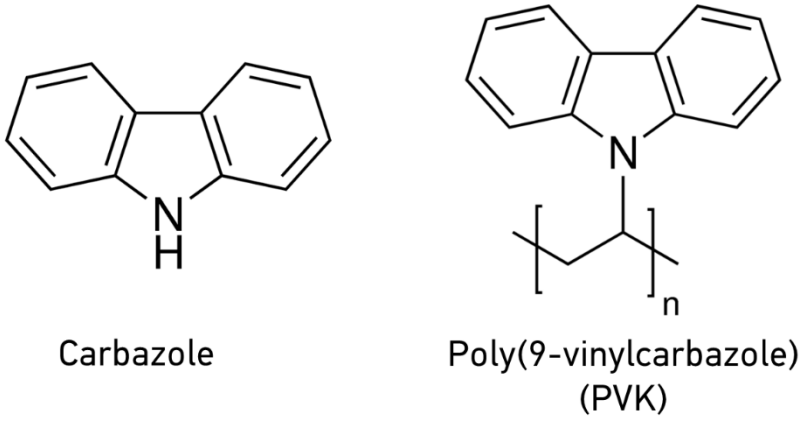

Fig. 1. Chemical structures of Carbazole and PVK

1.2. Organic semiconductors

Organic materials, which are used in various optoelectronic devices, such as OLEDs, organic solar cells (OSC) or organic field-effect transistors (OFET), are often called photo and electroactive materials as they are capable of light absorption, emission under UV or electrical excitation, generation and transport of charges from one electrode to other. Organic compounds with such properties are commonly referred to as organic semiconductors.

The organic materials are semi-conducting when the molecule consists of alternating single and double bonds. Such compounds are known as π-conjugated hydrocarbons and are the foundation of organic electronics. Unlike conduction in metals, organic semiconductors do not have free electrons but instead they are using shared electrons in a conjugated system therefore the transportation of charges is dominated by hopping between shared electron orbitals[9].

Carbon atom forms double bonds by sp^2 hybridization. In sp^2 hybridisation, one *2s* and two *2p* (p_x and p_y) orbitals are hybridized to form three strongly localized sigma (σ) bonds in a triangular flat structure with an angle of 120° among them. The third *2p* orbital (p_z) is still unhybridized. The p_z

orbital creates a π-bond only with another nearest p_z orbital, which is perpendicular to the σ-bond plane [10] (Fig. 2). The π-bonds are significantly weaker covalent bond type, compared to the σ-bonds.

For molecules which has conjugated double bond system, the electrons can be separated into two different sets: the strongly bound σ-electrons and the mobile π-electrons [11] which are delocalised and can easily hop from one molecule to another. That's why π-conjugated materials have fairly high conductivity and semiconducting properties [12].

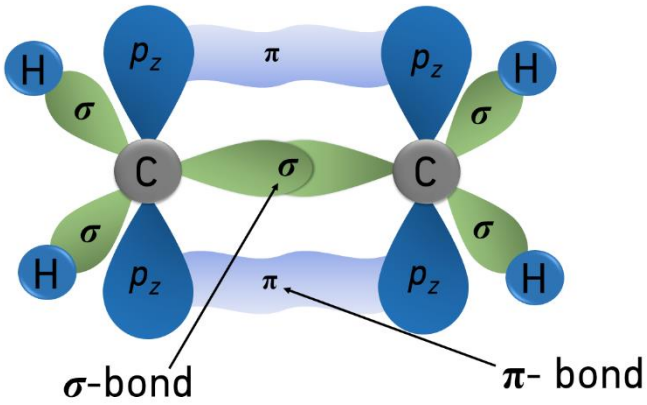

Fig. 2. Molecular orbitals of ethene. Overlapping p_z orbitals form the π-bond. Hydrogen atoms are connected to the C-atoms with σ-bonds

Also, π -conjugated materials have similar energy band structures to conventional semiconductors, which can be further explained by Molecular Orbital (MO) theory. According to it, the MOs become two semi-continuous bands of bonding (lower energy) and antibonding (higher energy) orbitals, forming the analogue to an inorganic semiconductor's valance and conduction bands [13] (Fig. 3), respectively. The Pauli exclusion principle declares that each energy state can be occupied by two electrons (spin up and spin down). Thus, in the ground state, just the bottom half of the energy levels are filled. The filled energy levels are covered by the highest occupied molecular orbital (HOMO) (π – bonding) and the empty levels begin at the lowest unoccupied molecular orbital (LUMO) (π^* – antibonding) (Fig. 3). The HOMO and LUMO are analogous to the top of the valence and the bottom of the conduction band, respectively [12]. So, delocalised electrons easily can be excited from HOMO to LUMO orbitals, this process is called $\pi - \pi^*$ transition [14].

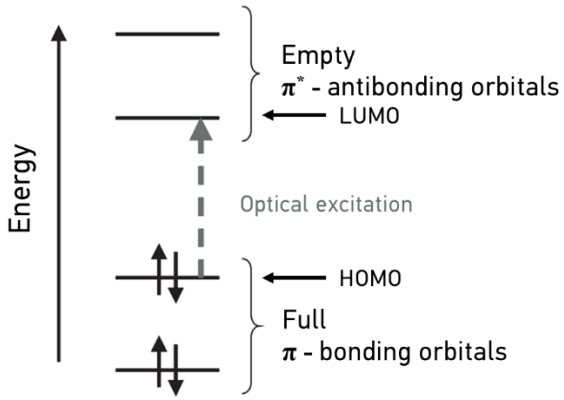

Fig. 3. Diagram of filled and empty HOMO LUMO energy levels. Figure adapted from *Shinar* [14]

The HOMO LUMO orbitals are extremely important because they are mainly responsible for many of the chemical and photo-physical properties of the molecule. According to *Koopmans'* theorem, the HOMO and LUMO energies of a molecular system equal to the ionization potential (I_p) and the electron affinity (E_a) of the molecule, respectively [11, 15]. The energy gap or the band gap $\Delta E_g = E_{HOMO} - E_{LUMO}$ is responsible for the optical properties of the molecule, e.g. absorption and emission. Whilst absorption and emission are actually intrinsic properties, charges are typically created on the outside, e.g. via injection by electrodes or dissociation of optically generated electron-hole pairs [16]. The HOMO LUMO gap can be adjusted by material engineering such as changing the number of aromatic rings or by incorporating different atoms like nitrogen, sulphur or oxygen. It makes possible for designing molecules with band gaps in the range between 1.5 eV (infrared) and 3.5 eV (ultraviolet)[9].

1.3. Organic semiconductors in excited state

1.3.1. Types of excitons

When organic molecule is excited optically or electrically, a hole and electron form a Coulomb-bound pair which is called an ***exciton***. The most common type of exciton in organic semiconductors is a *Frenkel* exciton. It is bound to the molecule with binding energy of 0.1 eV to 1 eV and is strongly localised in the molecule, unlike the *Wannier-Mott* excitons in inorganic semiconductors, where binding energies reaches just a few meV and are delocalised in order of tens of lattice constants [17]. In addition, a different class of excitons is often observed in organic materials - charge-transfer (CT) excitons, in which the electron is transferred to a nearest neighbour molecule. They are still localised and Coulomb-correlated, but because the charge separation is increased, the CT exciton binding energy is reduced. For electrical excitation, i.e. injection charges to an organic semiconductor, CT states are precursor states to the formation of intramolecular excitons [15]. Visualisation of exciton types can be seen in Figure 4.

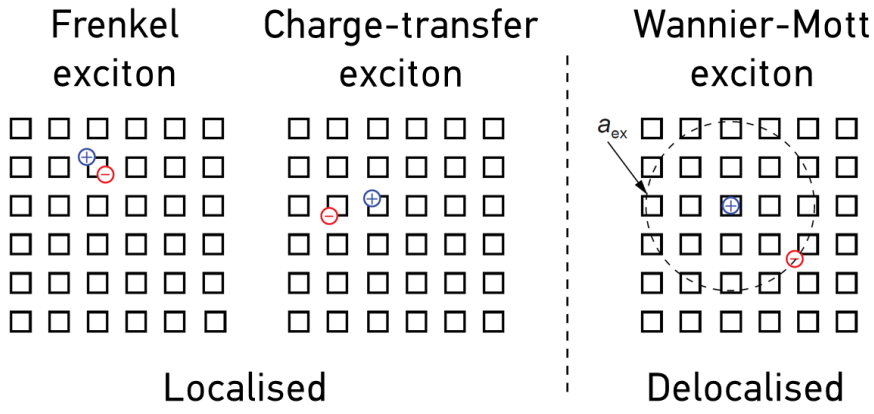

Fig. 4. Different types of excitons. a_{ex} stands for effective radius of *Wannier-Mott* exciton. Figure adapted from Reineke[15]

1.3.2. Formation of excitons

Monochromatic light absorption in an isotropic and homogeneous medium is described by the *Beer- Lambert law*:

$$A = \log\left(\frac{I_0}{I}\right) = \varepsilon c d, \tag{1}$$

Where *A* is a dimensionless unit, called *absorbance*, I_o - incident light intensity, *I* - transmitted light intensity, ε - molar attenuation coefficient of material, *c* - molar concentration of material and *d* - optical path length. So, following an exponential law, absorption reduces the incident light intensity I_o to $I = I(d)$ at a certain sample thickness *d* [15].

Absorption of light excites an electron from the HOMO (S_0 – *ground state*) to the LUMO (S_n – *excited state*). During optical excitation electron spin is preserved and only singlet excitons can be created, transitions to the triplet state are forbidden and excitons end up only in a singlet state. "Forbidden" is being used here in the typical quantum mechanical sense, which means that the probability of this process is orders of magnitudes lower than of those which are not spin-forbidden. The ratio of optically excited singlets/triplets in organic materials is the range of $10^9 - 10^{10}$ to 1 [18, 16].

Also, an excited state may be formed over electrical excitation that occurs in an OLED device configuration where the organic semiconductor film is inserted between two electrodes. Inversely to optical excitation, electrical excitation leads to the formation of both singlet and triplet states. Injected charges have statistically independent spin states, so by combining a pair of hole and electron, it can form either one singlet exciton state ($S = 0$) (upper-case letter is used to indicate the angular momenta of collections of particles) or one of three possible triplet exciton states ($S = 1$), so it has probability of 1/4 and 3/4, respectively [12].

During electrical excitation, an electron may be injected from the cathode into an empty π* LUMO and another electron is carried out by the anode from the full π HOMO thereby creating a hole. These charges drift through the solid until both live in the same or a nearby molecule and form a Coulomb-bound. The resulting configuration is that of an intramolecular or intermolecular excited state [19, 20].

To clarify the terminology, a singlet state is when the spin of electron ($s = \pm\frac{1}{2}$) in the LUMO and that of the remaining electron in the HOMO are anti-parallel (one is spin-up while other is spin-down or vice versa) and add up to a total spin of zero $S = 0$. The triplet state is when spins are parallel and add up to a total of one $S = 1$ [20]. Possible configurations of total electron spins in two particle system can be seen in Table 1.

Table 1. Possible configurations of electron total spin[16, 19]

Exciton	Spin wave function	*S*	*Ms*
Singlet	$\frac{1}{\sqrt{2}}\{\alpha_1\beta_2 - \beta_1\alpha_2\}$	0	1
Triplet	$\alpha_1\alpha_2$	1	1
	$\frac{1}{\sqrt{2}}\{\alpha_1\beta_2 + \beta_1\alpha_2\}$	1	0
	$\beta_1\beta_2$	1	–1

S – total spin, *Ms* – eigenvalue of the z-component of the spin, index 1 and 2 on α and β refer to electron 1 and 2.

The final spin of a state is provided by the combined total spin of all electrons in all orbitals. Need to take attention to the electrons in filled orbitals which are paired anti-parallel (sum of spins nullifies) so, they contribute zero to the total spin[19]. In Figure 5, the visual orbital configuration for the S_0 *(ground state)*, S_1 and T_1 states together with the resulting state diagram, can be seen.

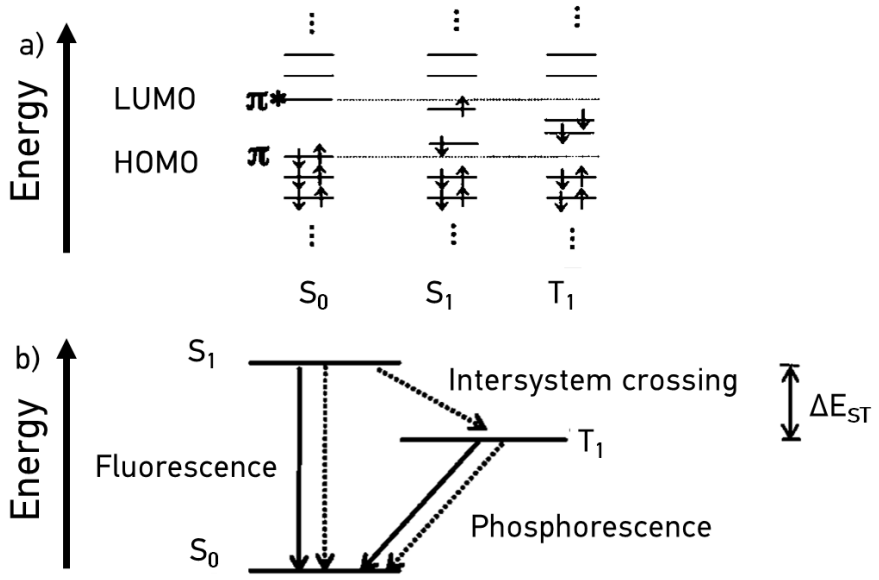

Fig. 5. a) Singlet and triplet states in an orbital configuration scheme. The arrows indicate the electron spin. For the triplet state, only one spin configuration is shown. b) Singlet and triplet states in a state diagram. Solid and dotted lines represent radiative and non-radiative decay channels. Figure adapted from *Köhler* and *Bässler* [19]

1.3.3. Excited state relaxation (Jablonski diagram)

All competing monomolecular photo-physical processes within an organic molecule that are involved in the excitation and de-excitation can be illustrated using the *Perrin–Jablonski* diagram [15, 21, 22, 16, 23] (Fig. 6).

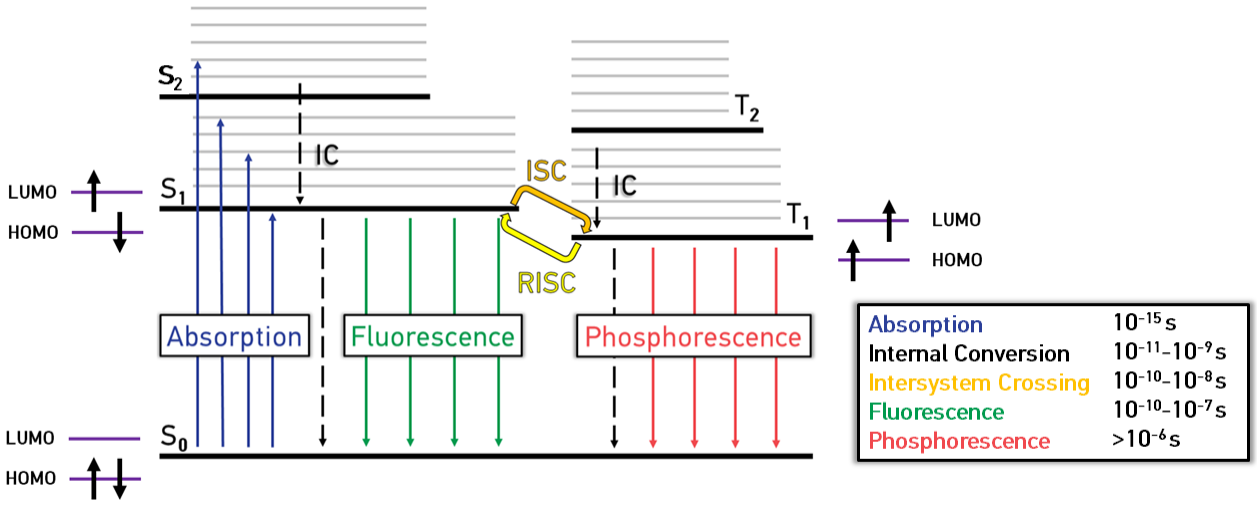

Fig. 6. The transitions between states are depicted as vertical lines. The thicker horizontal lines represent the electronic states and the thin lines are the vibrational states, where S_0 is the ground singlet state, S_1 is the first excited singlet state, T_1 the first excited triplet state. IC – internal conversion, ISC – intersystem crossing, RISC- reverse intersystem crossing. The spin configurations of the ground state, S_1 and T_1 are also shown in the diagram together with approximate time ranges for each process. Figure adapted from *Valeur* [21]

Jablonski diagram should be analysed from the beginning which is the light absorption (blue vertical line), it is without question the fastest process in this system (~10^{-15} s). Usually, at normal conditions, the vast majority of molecules are in lowest vibrational energy level of S_0, so absorption starts from this level and can bring an electron to one of the vibrational levels of S_1, S_2, …, S_n but usually they rapidly (10^{-11}–10^{-9} s) relax to S_1 without photon emission (non-radiative process), a transition is called *internal conversion* (IC) [23, 21]. After an exciton is formed, it can be followed by three different processes:

1. Radiative emission $S_1 \rightarrow S_0$ producing prompt fluorescence.
2. Non-radiative relaxation to the ground state - IC.
3. *Intersystem crossing* (ISC) to the triplet states.

Following the ISC, internal conversion (IC) relaxes to the lowest energy triplet state T_1 where excitons can have formally spin-forbidden radiative emission from triplet level – phosphorescence or again non radiative relaxation – IC. If small (< 0.1 eV) energy gap between S_1 and T_1 states exists, then additional spin flip back to the singlet state ($T_1 \rightarrow S_1$) is possible via *reverse intersystem crossing* (RISC) [23].

1.3.4. Types of radiative relaxation (Fluorescence and Phosphorescence)

According to Kasha's rule emissive recombination mostly occurs from the lowest excited state (S_1 or T_1) into the ground state (S_0) which tells us that there are two main types of radiative decay – fluorescence and phosphorescence [11, 24]. The difference between the two processes was originally made on the basis of the lifetime of the emission: in fluorescence, the duration of radiation is only in nanoseconds range, but in phosphorescence it is at least few orders of magnitude longer, mostly considered in microseconds to seconds range. In past decades the science behind emission radiation is largely improved and now the distinction is made based on their mechanisms: in fluorescence, the radiation is generated during transitions between states of the same spin multiplicity ($S_1 \rightarrow S_0$) and in phosphorescence, the radiation is generated by changing spin multiplicity ($T_1 \rightarrow S_0$) [20].

The fluorescence is a spontaneous process and its spectrum is shifted to longer wavelengths than the absorption spectrum (Fig. 7) because some of the initial excitation energy has been lost into the surroundings during vibrational relaxation. The gap (expressed in wavenumbers) between the maximum of the first absorption band and the maximum of fluorescence is called *Stokes shift* [21].

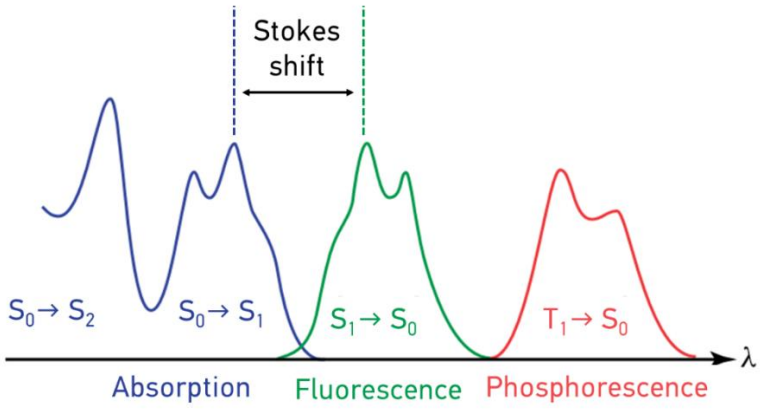

Fig. 7. Illustration of absorption, fluorescence and phosphorescence spectra along wavelength (λ) axis. Figure adapted from *Valeur* [21]

The phosphorescence transition ($T_1 \rightarrow S_0$) generally is forbidden process but it is possible to enable this transition by introducing a heavy atom such as iridium, osmium, europium, platinum to the organic molecule which introduce strong spin-orbit coupling due to their high atomic number Z[15, 16]. Strong spin-orbit coupling enables ISC ($S_1 \rightarrow T_n$) and that alters the probability of a triplet pair decaying to the ground state [9]. But typically, nonradiative de-excitation from the triplet state T_1 is still dominating in room temperatures or in non-rigid medium as solutions because of other competing mechanisms dominate over phosphorescence. In order to activate emissive radiation from triplets, rigid medium or low temperatures are required to surpass vibrational relaxation to S_1 [21]. Under such conditions, the lifetime of the triplet state may be long enough to observe phosphorescence on a time scale of seconds, minutes, or even more. The phosphorescence spectrum is located at wavelengths higher than the fluorescence spectrum (Fig. 7) because the energy of the lowest vibrational level of the triplet state T_1 is lower than that of the singlet state S_1 [21].

1.3.5. Delayed fluorescence

This brings us to third radiative de-excitation type – *delayed fluorescence* (DF) which is somewhere between fluorescence and phosphorescence in terms of lifetime of the emission and in terms of mechanism because it utilises both singlets and triplets [13].

As discussed previously about ISC ($S_1 \rightarrow T_n$), the opposite process, called *reverse intersystem crossing* (RISC) ($T_n \rightarrow S_1$) is possible if the energy difference ΔE_{ST} between singlet and triplet states are small enough (less than 0.1 eV) [23]. RISC is thermally activated process since triplet state lies below the singlet excited state and thermal energy helps to overcome small ΔE_{ST} energy gap by giving some energy to triplet states so it can be up-converted back to the singlet states [23]. This process is called *E-type delayed fluorescence* because it has been observed for the first time with eosin molecule [21] but also known as *thermally activated delayed fluorescence* (TADF). Recently, TADF mechanism gained a lot of attention because *Adachi* and co-workers published a series of articles [25, 26, 27] in 2009-2012, describing efficient molecular design strategies for TADF emitters. These papers made TADF so widespread that even today it is one of the most popular topics in OLED science field.

Alternatively, another type of delayed fluorescence exists which is called *P-type delayed fluorescence* (because it has been observed for the first time with pyrene molecule [21]) but also known as *triplet-triplet annihilation* (TTA). As the name suggests, it is a bimolecular process that occurs between two colliding triplet excitons [23]. Such a collision between two molecules in state of T_1 can supply enough energy to return one of them to the state of S_1, then TTA mechanism can result in DF and clearly increase the performance of OLED. The relaxation decay time of this type of TTA delayed fluorescence is half the lifetime of the triplet state in dilute solution, and the intensity has a characteristic quadratic dependence with excitation light intensity [21].

To summarise – the delayed fluorescence will have the same spectral shape as that of the prompt fluorescence, but with a significantly longer lifetime. Visualised mechanisms of TADF and TTA can be seen in Figure 8.

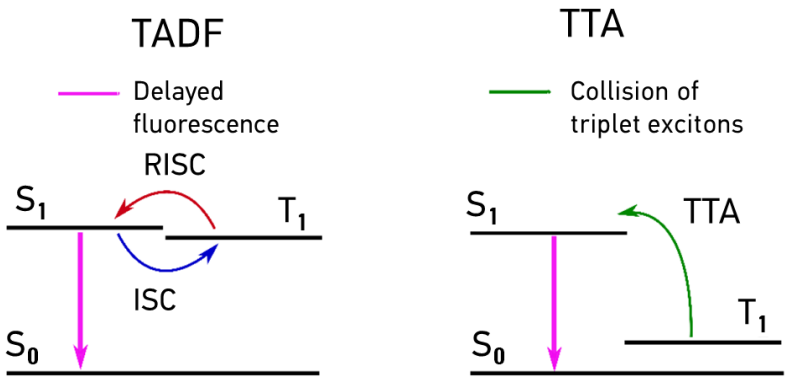

Fig. 8. Simplified schematic representation of the electronic energy levels involved in TADF and TTA mechanisms. Figure adapted from Dos-Santos [23]

1.3.6. Efficiencies of relaxation process

As discussed previously, according to spin statistics, electrically injected charges can form either a singlet or triplet excitons with probability of 1/4 and 3/4, respectively. Following this rule, on a fluorescent emitter, only the singlet excitons recombine radiatively and approximately 75% of the injected charge carriers are lost. Some could instinctively think that with phosphorescent emitter is vice versa – 75% relaxes radiatively and rest is lost but it is not quite right [16]. Strong spin-orbit coupling of phosphorescent materials leads to increased ISC ($S_1 \rightarrow T_1$) rate, therefore, the fraction of created singlets can be efficiently harvested for triplet state emission which makes it possible to reach 100% internal quantum efficiency of phosphorescence materials (Fig. 9), like reported by Adachi *et al.* [28] using iridium as heavy metal.

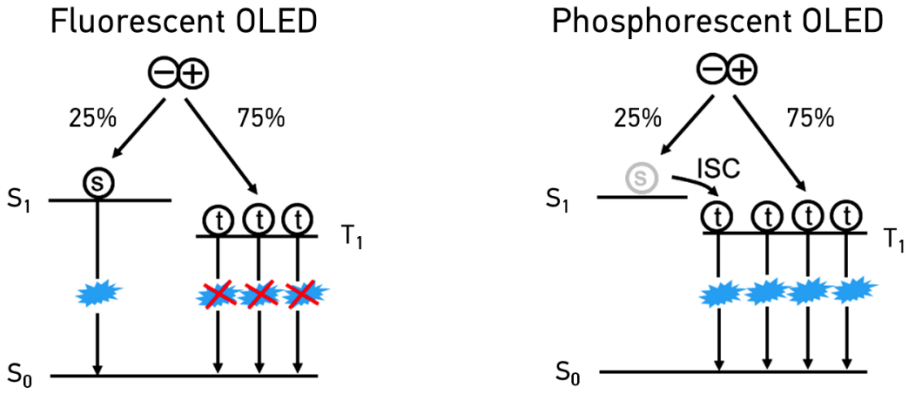

Fig. 9. Illustration of fluorescent and phosphorescent OLED excitons recombination behaviour. Figure adapted from Hoffman [16]

At first sight, phosphorescent emitter molecules appear to be the perfect candidate for high efficiency OLEDs, but new problems arise:

1. Phosphorescent emitters need to be doped into a suitable rigid matrix material, mostly to avoid concentration quenching and suppress vibrational relaxation [16].
2. Their long excited state lifetime causes a negative impact on the high brightness performance [15].

3. Because of the long lifetime, the triplet density inside the emissive layer can become extremely high in comparison to the singlet density in fluorescent OLEDs [16].

Therefore, many researchers try to improve OLEDs efficiency without drawbacks of phosphorescent materials and for this task *delayed florescence* (DF) materials comes in hand. As mentioned in section *1.3.5*, two main mechanisms of DF are TTA and TADF (Fig. 8). Because recombination of electrons and holes generated through electrical excitation results in a 1:3 ratio of singlet:triplets (Fig. 9), there is a 25% internal quantum efficiency limit imposed in fluorescent OLEDs and both mechanisms can help to overcome this limit [23].

TTA process is when two triplet excitons collide in order to gain enough energy to return one of them to S_1 state, this mechanism can result in DF and clearly increase the performance of OLED [29]. The maximum internal quantum efficiency of TTA is $25\% + \frac{1}{2} * 75\% = 62.5\%$ [30], where 25% is initial singlets formed and $\frac{1}{2} * 75\%$ is excitons converted from the triplet states.

TADF is another possible way to up-convert non-radiative triplet excitons to radiative singlet states and have a delayed emission. Basically, due to small ΔE_{ST} energy gap of TADF materials, heat energy is sufficient for accelerating RISC process (Fig. 8) and thus all 100% of excitons can be used for radiative emission at ideal conditions [27, 26, 25]. This process was well accepted by the scientific community and now TADF materials are very desirable for efficient OLEDs.

1.4. Fundamentals of Organic Light Emitting Diodes

Light-emitting diodes (LEDs) are known for almost hundred years. The first observation of LEDs was at 1927 by Russian scientist *Losev*, which studied the light emission from the point contact between a metal wire and a silicon carbide crystal, and recorded the spectrum of this light [31]. Today, LEDs is well known and widely used technology all around the world. You can find them almost at every lighting application such as general home or street lighting, LCD backlighted screens, flashlights, car headlights and etc [15].

The phenomena of electroluminescence from organic molecules are known already from 1950s but only at 1987 *Tang* and *van Slyke* [32] reported first practical OLED which induced lots interest from scientists in this field. Ever since this discovery, OLEDs managed to evolve from only laboratory tested ideas to huge market of high definition displays for smartphones or TVs [33]. In contrast to the traditional LEDs, which are mostly perfect point sources of light, OLEDs are area emitting devices and can be produced on flexible surfaces. Nowadays, typical OLED device is a multilayer structure of organic semiconductors sandwiched between electrodes, with a total thickness of only few hundreds nanometres [15]. The layer structure, working principles and other important parameters of OLEDs will be discussed in following sections.

1.4.1. Fabrication of OLED

Over a few decades of OLED investigation, two major techniques proved to be most efficient for fabrication of OLEDs: thermal evaporation in high vacuum and solution processing.

Thermal evaporation is probably the most popular method to fabricate OLEDs amongst both, scientists and factories. In this process, organic materials are placed in quartz crucible inside vacuum chamber with base pressure of 10^{-6}–10^{-7} mbar. Crucible is heated by tungsten coil until materials

starts to sublime. At the top of the vacuum chamber glass or plastic substrates are put in holder which constantly rotates to ensure it deposits evenly. The rate of the deposition is monitored by a quartz crystal resonator monitor and controlled by changing the temperature of heated material. Several shutters are used to both control the exposed substrate area or to cover the material source [9].

Thermal evaporation helps to produce reliable and highly efficient multi-layered devices but there are some limitations - only small molecule materials can be thermally evaporated, because polymers are chemically degrading at high temperatures even before they could technically evaporate. Even though small-scale production of single OLEDs for research purpose is quite easily achieved, big scale production is difficult and expensive due to huge (for example TV sized) vacuum chambers required and difficulties to make layers evenly distributed within large area [15].

Solution processing is useful method for using polymer materials to make OLEDs

Polymer OLEDs are mostly fabricated utilizing solution processing techniques, like the spin coating. However, even some small molecule organic semiconductors have demonstrated quite good properties in solution-processed devices [34]. Moreover, using small molecules to create white solution processed OLEDs is the main topic of this work.

In solution processing, organic materials are dissolved in appropriate solvent and dispensed onto the prepared substrate. The substrate is then spun at high speeds (500–4000 rpm) in order to throw off excess material, leaving evenly distributed thin (30–60 nm) film (Fig. 10). Film thickness can be controlled by using different spin speed, different concentration of material in solvent and even changing solvents with different evaporation rate. The final thickness is usually reached just after 20 seconds, but the substrate is still spun for 40–60 seconds to further dry the film. Then the films are annealed in order evaporate residual solvent trapped inside the layer [12]. The annealing temperature is kept below the glass transition temperature of the material, so that the film remains amorphous [9].

Regardless of the fabrication techniques, all OLEDs must be fabricated in an inert atmosphere with very low oxygen and humidity level [2].

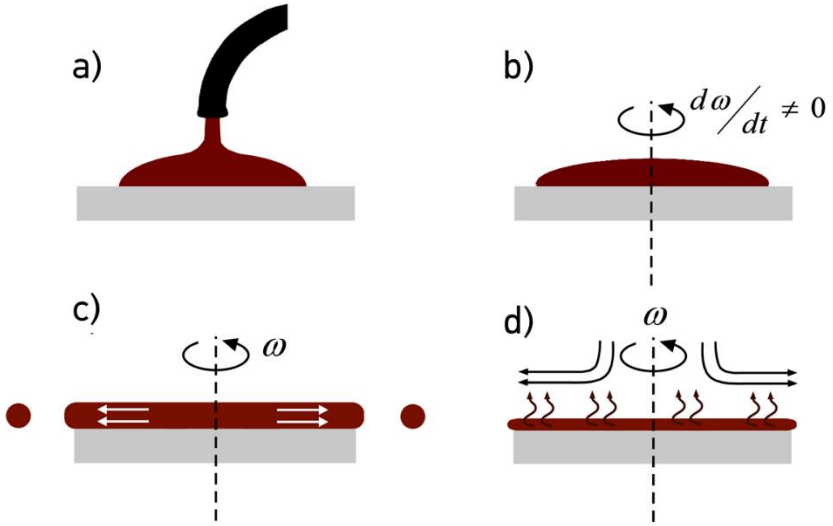

Fig. 10. The different "stages" of spin coating process: a) dispensation, b) acceleration, c) flow dominated, d) evaporation dominated. Figure adapted from [35]

1.4.2. Principles of OLED operation

As mentioned earlier, first OLED devices had really simple structure, which consisted only from thin organic film sandwiched between two metal electrodes. Nowadays, OLEDs are made up of stack of organic layers (3–8 layers) with a particular function in mind, sandwiched between anode and cathode which inject holes and electrons, respectively. After traveling through various layers, charges recombine in *emissive layer* (EML) and photons are radiated [23]. Typical OLED structure is shown in Figure 11.

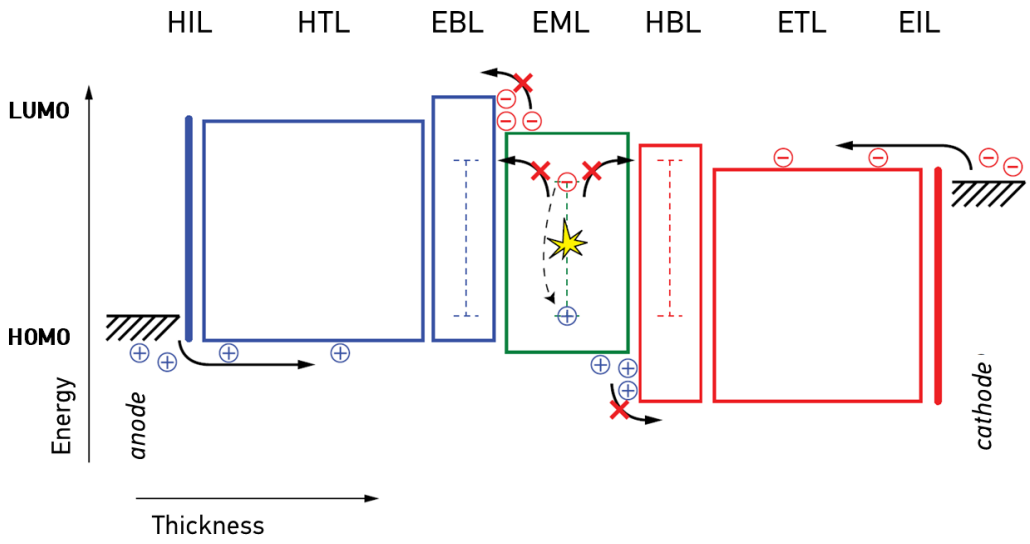

Fig. 11. Energy diagram of a typical multilayer OLED. From anode to cathode there are the hole-injection layer (HIL), the hole-transport layer (HTL), the electron-blocking layer (EBL), the emission layer (EML), the hole-blocking layer (HBL), the electron-transport layer (ETL), and the electron-injection layer (EIL). Boxes indicate the highest occupied (HOMO) and lowest unoccupied (LUMO) molecular orbital levels of the materials. The dashed lines in the EBL, EML, and HBL are the desired triplet energies of the materials in the case of phosphorescent OLEDs. Figure adapted from *Reineke* [2]

Injection of holes into the device occurs via the anode layer, and indium tin oxide (ITO) is the most widespread anode used in OLEDs. It is one of the most frequently used transparent conducting material due to its good electrical conductivity parameters and optical transparency [23]. The cathode is responsible for the injection of electrons into the device. Most widely used cathode is Aluminium (Al) due its good availability, low price and ease of use, however, this comes at a price: Al has a relatively high work function which need to be overcome by using additional layer – electron injection layer (EIL).

Most commonly used EIL is a thin layer (~1 nm) of *lithium fluoride* (LiF) incorporated between organic layers and Al. LiF layer reduces the electron injection barrier at the Al-organic layer interface [36]. In similar manner, thin layer MoO_3 is used on top of anode ITO layer as hole injection layer (HIL).

The hole transport layer (HTL) takes all injected holes from HIL and, as the name suggests, transports them further into OLED structure while electron transport layer (ETL) do the same but for electrons and from the cathode side. Good example for popular HTL and ETL materials would be *N,N'-Di(1-naphthyl)-N,N'-diphenyl-(1,1'-biphenyl)-4,4'-diamine* (NPB) and *2,2',2''-(1,3,5-Benzinetriyl)-tris(1-phenyl-1-H-benzimidazole)* (TPBi), respectively.

The hole blocking (HBL) and electron blocking (EBL) layers not only helps to keep injected charges only in EML but also moderately decrease energy barrier between transport and emissive layers which ensures smooth transition between layers and helps with efficiency [13]. As a rule of thumb, good HBL have low HOMO level and/or low hole mobility. Idea is also the same with EBL – high LUMO and/or low electron mobility [23]. Purpose of blocking layers demonstrated visually in Figure 11.

Finally, EML is where all transported holes and electrons recombine and emit photons. EML can be either pure emitters or host:guest system, where the light-emitting material is doped with a low concentration (<10 %) into a host. Generally, host is an organic material with good charge mobility and a band gap wider than the emitting guest. Using host:guest system allows to avoid concentration quenching effects and ensure high emission efficiency of OLED [33].

Additionally, when choosing materials for OLEDs, some basic rules should be checked:

- Materials should be morphologically stable and form uniform films;
- The HOMO-LUMO energy levels of each layer should be ideally aligned depending on their specific function in the device;
- The triplet energy of the layers should be checked in order to prevent exciton quenching, especially in layers close to the emissive layer;
- The carrier mobility of each layer should be suitably adjusted by optimising the thickness of each layer in order to get good charge carrier balance [23].

1.5. OLED parameters

Before discussing and analysing certain parameters of OLED, some physical terms needs to be defined briefly. OLEDs, including many other light-emitting devices, are typically characterised by photometric quantities, which include brightness, and its synonym luminance. Photometry, in comparison to the radiometry, quantifies light parameters of different wavelength in a different way, according to the sensitivity of the human eye. Photometric quantities ensures that light sources of different colour, which appear equally bright to the eye of observer, will have the same amount of brightness [15].

1.5.1. Parameters of human eye

In order to better understand this concept, it is beneficial to remember course of human eye anatomy from high school classes (Fig. 12). The light emitted from the source and what humans perceive is not the same, it depends on specific eye anatomy and how this information is processed in the brain. Light which is going to the eye, firstly hits cornea, iris, and the lens until it finally reaches the retina. Inside the retina, there are only two types of photoreceptor cells: rods and cones. Rods are mainly sensitive to very low light intensity and provide black and white vision (scotopic vision). Then again, there are three types of cones (long-, medium- and short-wavelength) which are responsible for the perception of colour in bright environment (photopic vision) [16].

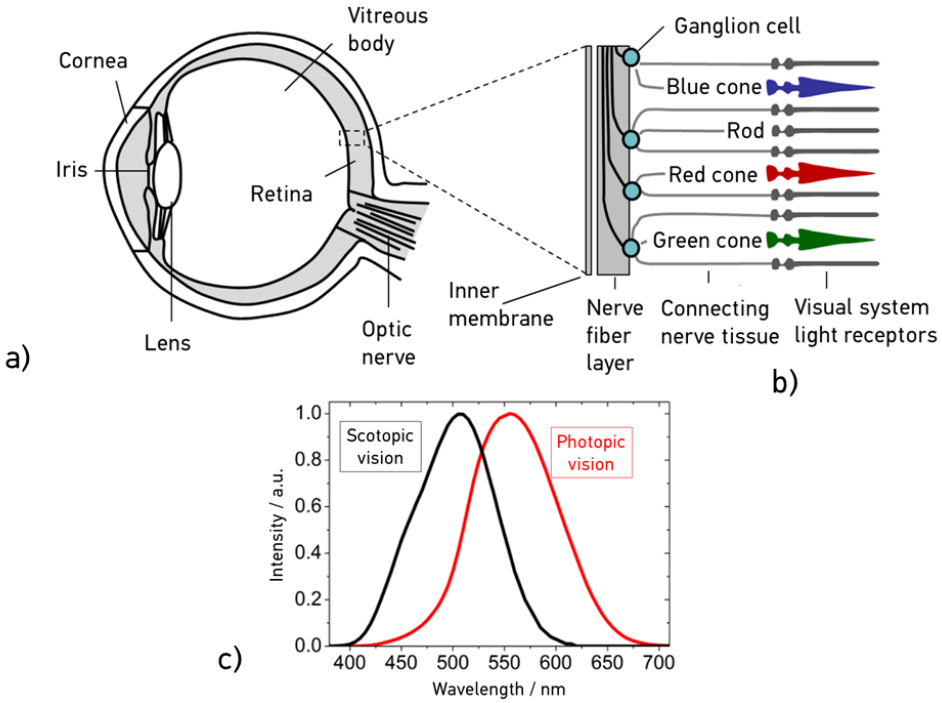

Fig. 12. The anatomy of the human eye (a) and the detailed structure of the retina (b). Rod and cone photoreceptor cells lead to two luminosity function curves (c) which describes the sensitivity of the eye to the different wavelengths. Figure adapted from *Hofmann* [16]

Due to the two different types of photo reception cells, there are respectively two luminosity functions which describes the human eye sensitivity to the light of certain wavelength. Those two functions are called the photopic function ($V(\lambda)$) and the scotopic function ($V'(\lambda)$) (Fig. 12 c) [16]. Both functions are provided by the *Commission Internationale de l'Eclairage* (CIE) [37].

1.5.2. Photometry units

As discussed in previous section, the human eye is most sensitive to the green colour with wavelength of $\lambda = 555$ nm and the perception goes down with the change of wavelength on either side of the peak (Fig. 12 c). This means that the perception of human eye at UV region ($\lambda = 380$ nm) is almost zero.

As a result, a green OLED will have much bigger brightness when compared to blue OLED, even though they are emitting the same amount of power [12]. For clarification, units which are adjusted to reflect human eye sensitivity and describes OLED parameters will be discussed:

- Luminous flux or luminous power (*SI unit: lumen, lm*) is defined as total photometric power emitted in all directions from a light source. In other words, it is photometrically weighted radiant flux or power (*SI unit: watt, W*) [38, 39].
- Luminous intensity (*SI unit: candela, cd*) is power emitted by a light source in a specific direction, weighted by the photopic function, basically, takes into account the colour of the light and its direction. It is photometrically weighted radiant intensity (*SI unit: watt per steradian, W/sr*) [38, 39].

Finally, the illuminance and the luminance, which are the luminous flux and luminous intensity per unit of area, respectively.

– Illuminance (*SI unit: lm/m^2 or lux, lx*) measures how much incident light illuminates the surface [38, 39].
– Luminance (*SI unit: cd/m^2*) measures of how "bright" a surface appears when we view it from a given direction. It is photometrically weighted radiance (*SI unit: W/m^{2}sr*) [38, 39].

1.5.3. External quantum efficiency

Units discussed in previous section are helpful for describing brightness and efficacies, such as current efficacy (*SI unit: cd/A*) or power efficacy (*SI unit: lm/W*) but all of those are adjusted to eye sensitivity.

***Note**: Efficacy should not be confused with efficiency. Efficacy represents ratio of 2 different units i.e. power efficacy in lm/W tells us how many lumens we get from 1 watt of power. Efficiency is dimensionless quantity which represents ratio in between single unit, i.e. power efficiency would be a ratio of how much power we get vs. how much power we put in (i.e. light bulb emits 5 W of optical power while it consumes 10 W of electrical power, 5/10 = 0.5, this means light bulb power efficiency is 50%).*

If we want to compare OLEDs independently from eye sensitivity or spectra it produces, we need to calculate *external quantum efficiency* (EQE) which can be described as a ratio of photons which are emitted forwards to the injected electrons [9, 12, 13, 16, 15, 38]. EQE can be express ed with such formula:

$$EQE = IQE \cdot \eta_{OUT}; \quad (2)$$

where IQE is internal quantum efficiency and η_{OUT} is outcoupling efficiency. The IQE can be expresses as:

$$IQE = \gamma_{bal} \cdot r_{ST} \cdot \Phi_{PL}; \quad (3)$$

where γ_{bal} is the charge balance factor, which is ideally equal to 1 (the same amount of holes and electrons injected). The r_{ST} is ratio of generated radiative excitons. As discussed previously, singlet:triplet excitons are generated in ratio of 1:3, this means, that for fluorescent emitter, which utilises only singlet excitons, $r_{ST} \leq 0.25$. If emitter can utilise 100% of singlet and triplet excitons (phosphorescent or TADF material), then $r_{ST} \leq 1$. The Φ_{PL} is *photoluminescence quantum yield* (PLQY) which is characteristic property of emitter. PLQY can be simply described as the ratio of the number of photons emitted to the number of optically absorbed photons, which is ideally close to 1 [22]. It can be easily seen, that even at ideal case, fluorescent emitter can have only 25% of IQE, while phosphorescent and TADF materials can reach 100% of IQE.

Light outcoupling η_{OUT} could be described as ratio of number of photons emitted forwards from OLED to the number of all generated photons. Unfortunately, due to OLED architecture, a huge fraction of generated photons cannot escape to the air. Mechanism of light propagating inside OLED can be seen in Figure 13.

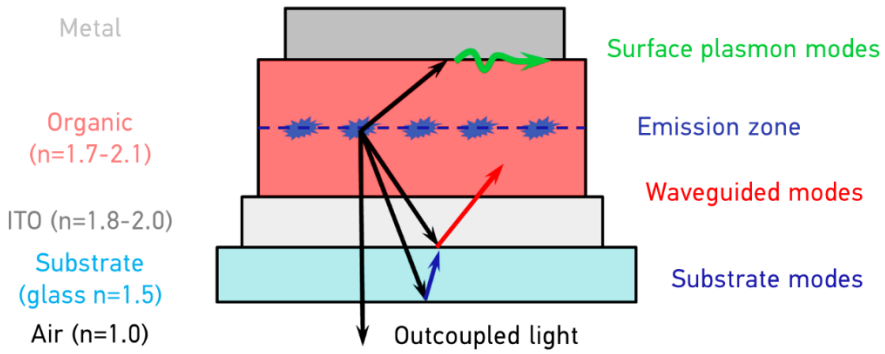

Fig. 13. Simplified mechanisms of light loss inside OLED. Figure adapted from *Hofmann* [16]

Light outcoupling can be expressed using simplified formula [40, 41]

$$\eta_{OUT} = \frac{1}{2n^2} \tag{4}$$

where *n* is the refractive index of the glass substrate. Therefore, if standard glass has *n = 1.5*, then the η_{OUT} roughly is around 20%. This means, that theoretically even if IQE is 100%, the optics of OLED only allows 1/5 of generated photons to escape into the air [15, 2]. Fortunately, in practice, it is possible to reach much higher outcoupling efficiencies. It is very complicated mechanism and even small changes such as horizontal or vertical orientation of emissive layer dipoles can have a huge impact and help to reach $\eta_{OUT} = \sim 36 - 38\%$ [42, 43]. Also modifying a glass substrate surface by adding a lens or array of micro lenses can improve outcoupling. Thus said, researchers managed to reach high values of EQEs and records at this moment are ~31% for solution processed OLED [44], ~37–38% for vacuum processed OLED [42, 43] and even more than 50% when combining very efficient OLEDs with thin external scattering layer which helps to extract more photons to air [45].

1.5.4. Colour parameters

When discussing about OLEDs, one more group of parameters should not be forgotten. It is optical parameters which helps to evaluate the quality of colour it produces: *Commission Internationale de l'Eclairage* (CIE) chromaticity coordinates, the *correlated colour temperature* (CCT) and the *colour rendering index* (CRI).

Almost 100 years ago it was a hard task to discuss about colour of an object or light source. Especially when there was a mix of essential colours red, green, blue (RGB). One could describe a mix of green and blue colours as greenish-blue, bluish-green, or sky-blue which was confusing. In order to make those discussions scientifically correct, in 1931 CIE came in help and introduced a two-dimensional, horseshoe shaped chromaticity diagram which plotted all possible combinations of RGB colour mix [46, 37] (Fig. 14).

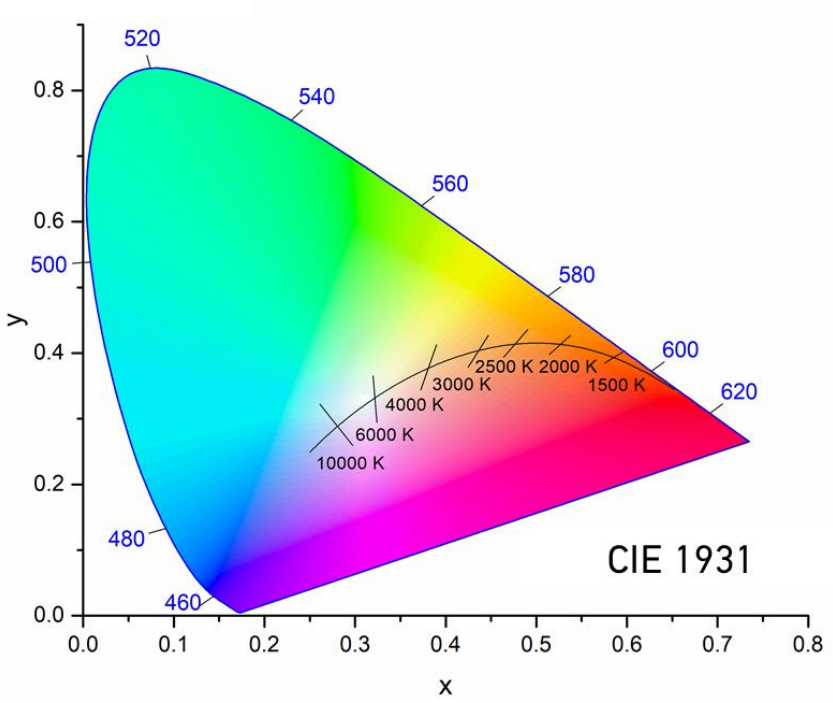

Fig. 14. CIE 1931 chromaticity diagram with Planckian locus

These coordinates (*x, y*) can be obtained from tristimulus values *X*, *Y*, *Z* which are calculated from spectral distribution colour matching functions [47, 16]:

$$x = \frac{X}{X+Y+Z}, \qquad y = \frac{Y}{X+Y+Z}; \tag{5}$$

White light, which is used for inside lighting of buildings, should be similar to a blackbody radiator and be close to the ideal white point which is (*0.33, 0.33)* in CIE 1931 chromaticity diagram.

Differently than incandescent light bulbs, LED and OLED emits light not from thermal radiation of hot filament, but the shade and tone of white light is still described in temperature units – Kelvin (K). CCT is based on blackbody radiator model and counterintuitively - the higher is the colour temperature, the cooler the white light will be [3, 38]. Incandescent bulbs are usually around 2700–3000 K range, which is a "warm" light, while a cool white light LED has a CCT of 6500 K. Incandescent bulbs CCT are best suitable for interior application, while others applications require higher CCT, i.e. factories, parking lots, warehouses require 3700–4000 K to be more neutral lighting, retail stores uses colder white light of 5000–6500 K and very high CCT of 8000–10 000 K can be used in aquarium applications [47]. If compared to the natural sunlight, then sunset/sunrise would correspond to 3200 K and a sunny day would be close to 5800 K of CCT[16].

Besides the CIE and CCT, another parameter to characterise the quality of white light is *colour rendering index* (CRI), which is used to describe the ability of light source to accurately render all colours in illuminated space [47]. The CRI of a light source is measured in range between 0 and 100. The higher the CRI value, the stronger the ability to reproduce the true colour of illuminated objects (Fig. 15). For example, general lighting sources with the CRI of 80 and above are considered to have good colour rendering properties, while incandescent bulbs and sunlight have CRI of 100.

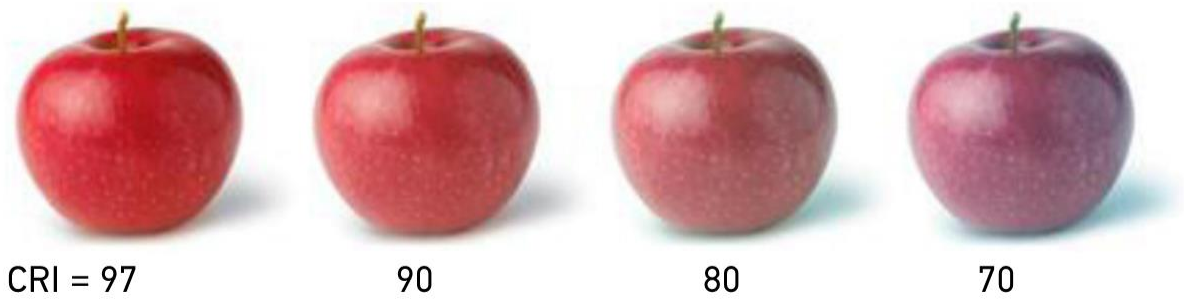

Fig. 15. Demonstration of the visual effect for different CRI values at CCT = 2700 K. Figure adapted from[47]

1.6. White colour hybrid OLEDs

Typically, white OLEDs have been grouped into three categories based on the emitters used, such as all-fluorescent, all-phosphorescent and third − hybrid white OLEDs which is a promising approach to achieve white colour emission with high efficiency and long lifetime by combining emissions from blue fluorescent and long wavelength phosphorescent emitters. Therefore, hybrid approach is ideal option because of their unique advantage of harvesting both singlet and triplet excitons, which leads to theoretical IQE of 100% [48, 49]. Lately, some interesting methods have been suggested for producing white hybrid OLEDs based on a phosphorescent emitter as a guest and either fluorescent or even TADF emitters partially acting as the hosts [50, 51, 52, 53]. For example, Miao and Wang *et al.* developed white hybrid multi-layered (>10 layers) OLEDs with high CRI values by utilising complicated four component emission from three phosphorescent and one fluorescent emitters [49]. Performance and colour properties comparison of white colour hybrid OLEDs produced with different approach to emissive layer composition are given at Table 2.

Table 2. Performances of the representative white hybrid OLEDs

Ref	Emissive layer composition	V_{ON}, V	EQE_{max}, %	CIE 1931 (x, y)	CRI	CCT, K
53	Single emissive layer[a]	3.19	15.0	(0.348, 0.422)	63	5990
53		3.11	19.1	(0.358, 0.430)	54	4155
53		3.06	20.8	(0.398, 0.456)	48	3671
52	Double emissive layer[a]	3.7	2.8	(0.353, 0.380)	77.1	4829
52		3.6	2.7	(0.279, 0.364)	77.5	7861
51		4.06	8.91	(0.380, 0.431)	50	4390
51		4.60	7.95	(0.369, 0.401)	60	4905
49	Seven ultrathin layers system[a]	3.3	19.34	(0.482, 0.430)	96	2559
49		3.3	18.40	(0.427, 0.462)	85	3579
49		3.3	18.82	(0.464, 0.430)	90	2789
49		3.3	17.82	(0.505, 0.412)	85	2190
54	Single emissive layer[b]	2.8	22.7	(0.41, 0.43)	-	3509
54		2.8	22.9	(0.38, 0.41)	-	3968,
55		3.8	21.0	(0.43, 0.43)	70	-

[a] devices prepared by vacuum deposition, [b] devices prepared by solution processing

All in all, white colour hybrid OLED is a promising technology for lighting and display industry, which actively attracts attention of scientist all over the world, because organic semiconductors, combined with modern material engineering, offers endless possibilities for device optimisation in terms of colour, efficiency, lifetime, etc. Therefore, in this work, aiming to achieve high value of CRI

with emission close to the natural white with CIE coordinates of (0.33, 0.33) or to get human eyes friendly electroluminescence with CCT value close to 3000 K, approaches for fine tuning of colour properties of solution-processed white hybrid OLEDs were developed by utilising a strategy of single hybrid emissive layer with ultralow concentrations of phosphorescence iridium (III) complexes and TADF compounds as emitters with high light-emissive exciton recombination probability (theoretically 100%).

2. Materials and Experimental methods

2.1. Materials

In this work, properties of two phosphorescent iridium (III) complexes, shortly named **Red** and **Orange** were investigated (Fig. 16). Emitter *bis(2-(benzo[b]selenophen-2-yl)pyridinyl) Ir(acetylacetonate)* (**Red**) was synthesised by a scientific research group, which is supervised by Dr. Pavel Arsenyan, Latvian Institute of Organic Synthesis [56]. Second emitter *bis(2-(4-bromophenyl)-6-methyl-4-phenylquinolinyl)Ir(2-(2-pyridyl)benzimidazole)* (**Orange**) (Fig. 16) was synthesised by a scientific research group, which is supervised by Dr. Sathiyanarayanan Kulathu Iyer, Vellore Institute of Technology, India [57].

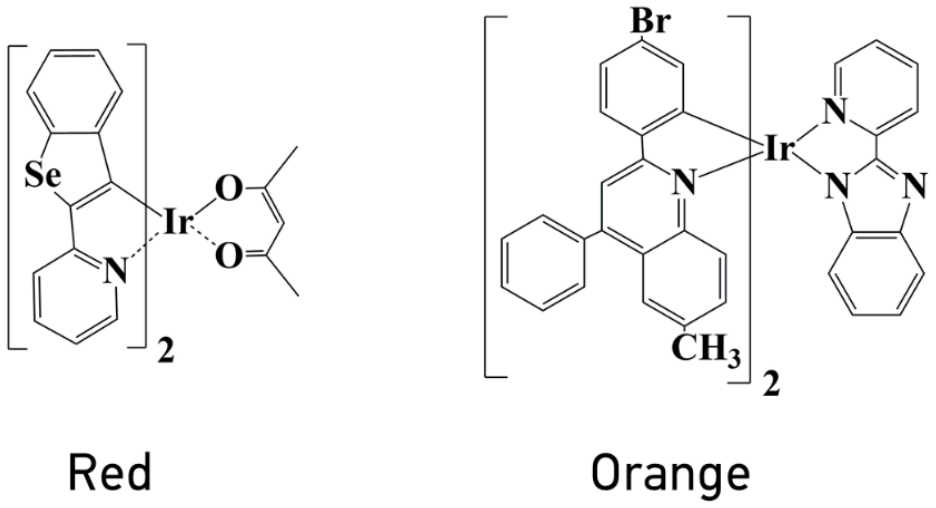

Fig. 16. Chemical structure of **Red** and **Orange** emitters.

For fabrication of devices, *molybdenum trioxide* (MoO_3), *N,N'-Di(1-naphthyl)-N,N'-diphenyl-(1,1'-biphenyl)-4,4'-diami*ne (NPB), *tris(4-carbazoyl-9-ylphenyl)amine* (TCTA), *1,3-bis(9-carbazolyl)benzene* (mCP), *diphenyl-4-triphenylsilyl-phenylphosphineoxide* (TSPO1) and *2,2',2''-(1,3,5-benzinetriyl)-tris(1-phenyl-1- H-benzimi-dazole*) (TPBi) were purchased from *Sigma-Aldrich* and used as received.

First green TADF emitter *9-[4-(4,6-diphenyl-1,3,5-triazin-2-yl)phenyl]-N,N,N',N' -tetraphenyl-9H-carbazole3,6-diamine* (DACT-II)[58] were bought from *Xi'an Polymer Light Technology*[59]. Second green TADF emitter *4,6-di(9,9-dimethylacridan-10-yl)isophthalonitrile* (DAcIPN) were synthesised by Dr. Eigirdas Skuodis[60], Department of Polymer Chemistry and Technology, Kaunas University of Technology.

HOMO LUMO energy levels of used organic compounds are given in Table 3, chemical structures are depicted in Figure 17.

Table 3. HOMO LUMO values of organic compounds used in OLEDs production

Material	HOMO, eV	LUMO, eV	Reference
NPB	5.5	2.4	[61]
TCTA	5.7	2.4	[62]
mCP	5.9	2.4	[63]
TSPO1	6.8	2.5	[64]
TPBi	6.2	2.7	[65]
DACT-II	5.5	3.2	[58]
DAcIPN	5.65	3.3	[60]

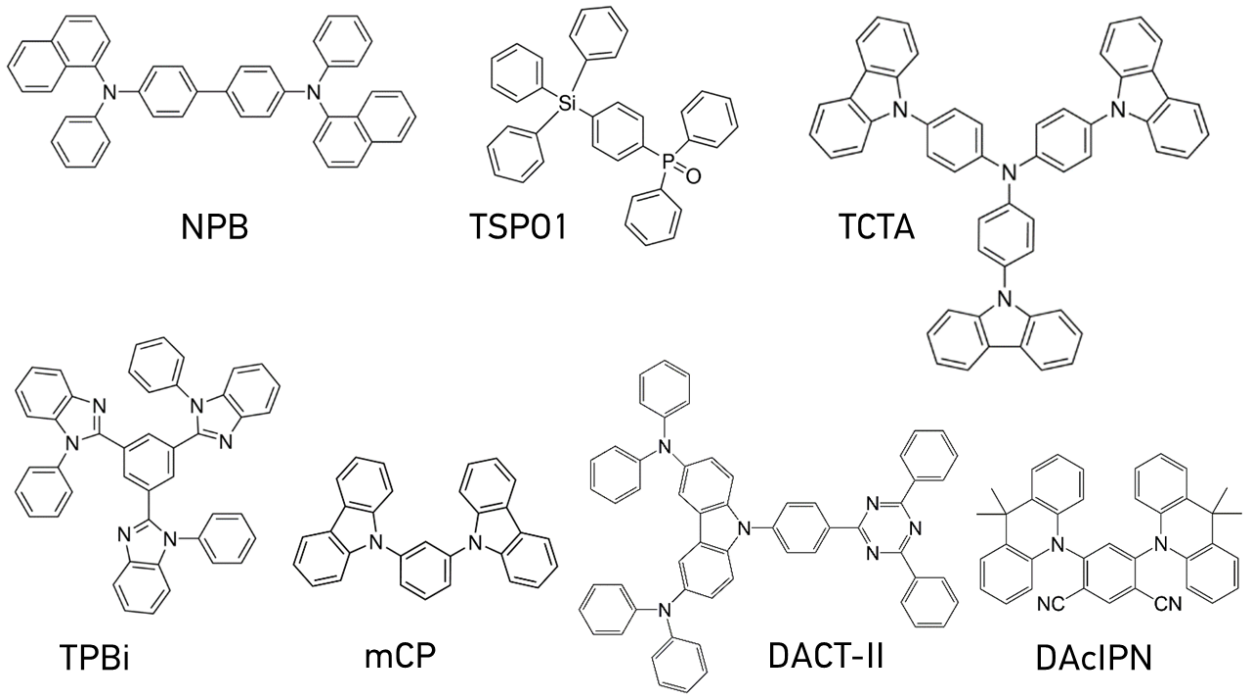

Fig. 17. Chemical structures of organic compounds used in OLEDs production

2.2. Experimental methods

Absorption and photoluminescence spectra of investigated compounds were recorded using *Avantes AvaSpec-2048XL* and *Edinburgh Instruments FLS980* spectrometers, respectively (Fig. 18). Dilute solutions (10^{-4}–10^{-5} M) of compounds were measured in standard quartz cuvettes. Thin film samples were prepared either by spin coating from a solution or by vacuum deposition on to quartz substrate. For measuring photoluminescence, samples were excited by xenon lamp at the wavelength of 350 nm. PLQY of solutions and thin films were estimated using integrated sphere accessory to *Edinburgh Instruments FLS980* spectrometer. Photoluminescence decay curves of samples were obtained utilising a time-correlated single photon counting technique, while exciting sample with a *PicoQuant LDH-D-C-375* diode laser (excitation wavelength of 374 nm), coupled to FLS980.

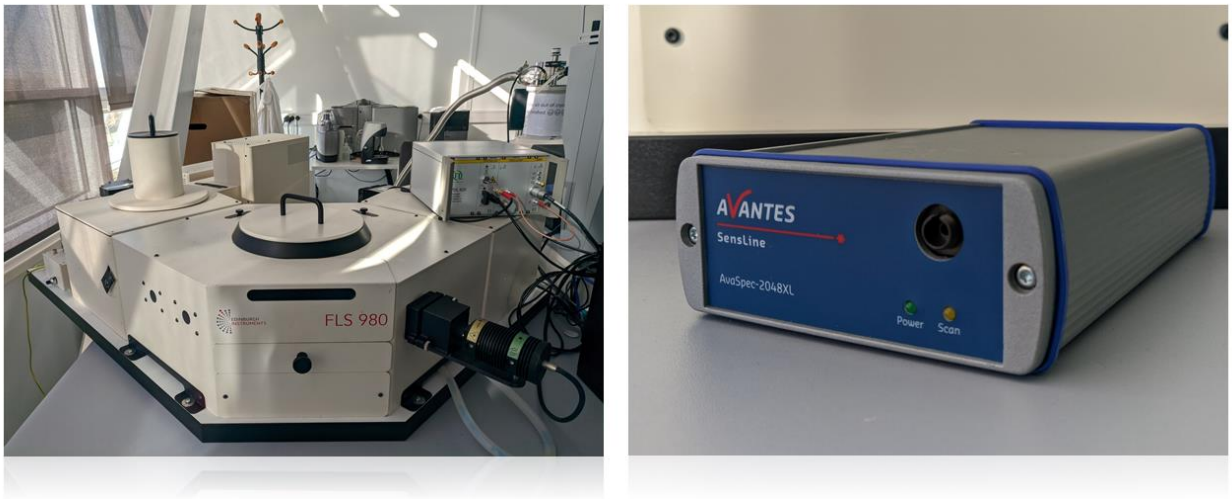

a) b)

Fig. 18. *Edinburgh Instruments FLS980* photoluminescence (a) and *Avantes AvaSpec-2048XL* UV-Vis (b) spectrometers

The cyclic voltammetry (CV) measurements were carried out by using a three-electrode assembly cell and a *μ-AUTOLAB Type III* potentiostat-galvanostat. Glassy carbon (a disk diameter of 2 mm) was used as working electrode, a silver wire was utilized as potential reference electrode and platinum wire as a counter electrode. The solutions of samples had the concentration of 10^{-3} M in dry, argon purged dichloromethane containing 0.1 M tetrabulthylammonium hexafluorophosphate ($TBAPF_6$) as supporting electrolyte. The measurements were taken at a constant 50 mV/s potential rate at room temperature. At the end of the measurements, ferrocene (Fc) was added as internal reference. Ionization potential (I_P^{CV}) was estimated from the onset oxidation potential using the relationship:

$$I_P^{CV} = 4.8 + E_{ox}vs.Fc; \quad (6)$$

where $E_{ox}vs.Fc$ is the onset of first oxidation potential versus the Fc reference.

The ionization potentials (I_P^{PE}) for solid state of investigated materials were recorded by the electron photoemission spectrometry. Setup of the IP measurements consisted of monochromator (*CM110 1/8m*), 30 W deep UV deuterium lamp (*ASBN-D130-CM*) and electrometer (*Keithley 6517B*). Samples for measurements were prepared by vacuum deposition on to clean fluorine doped tin oxide (FTO) coated glass. Energy scan of the incident photons was performed while increasing the incident photon energy by changing wavelength with monochromator from 280 to 180 nm in steps of 1 nm. Resulting photocurrent was registered by electrometer. The I_P^{PE} values were taken from intersection of x- axis and the low energy linear part of measured photoelectron emission spectra.

Electron affinities (E_A^{PE}) of thin films were estimated using formula:

$$E_A^{PE} = I_P^{PE} - E_g; \quad (7)$$

where E_g is the optical bandgap, taken from onset of lowest energy absorption band using *Tauc* relation as described by *Swart et al* [66]

Vacuum processed OLEDs were made using *Kurt J. Lesker* vacuum equipment which is in-built in *MB EcoVap4G* glove box with inert atmosphere of nitrogen (Fig. 19). Layers were deposited on to indium tin oxide (ITO) coated substrates under vacuum higher than $2 \cdot 10^{-6}$ mbar. ITO coated glass substrates with a sheet resistance of 15 Ω/sq were pre-patterned for getting seven independent devices with area 6 mm^2. Surface substrates were cleaned by sonicating 10 minutes in pure acetone following by 10 minutes in isopropyl alcohol and dried by nitrogen gun, then substrates had 15 minutes UV ozone treatment in device made by *Ossila* company.

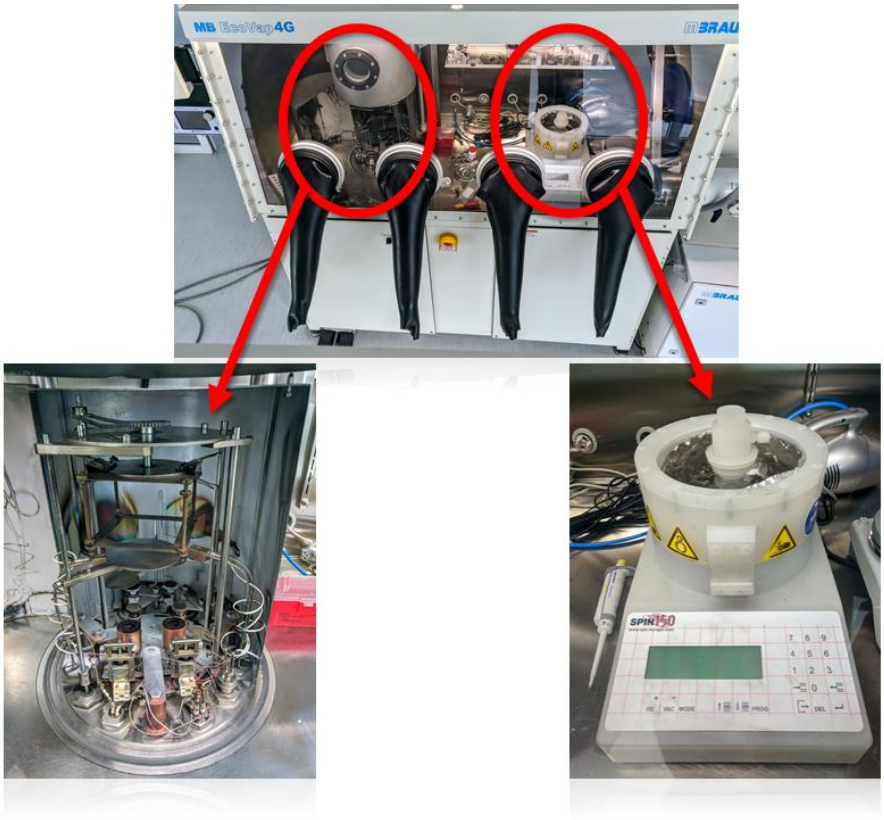

Fig. 19. *MB EcoVap4G* glove box (top) with inside mounted *Kurt J. Lesker* vacuum deposition chamber (left) and *SPS Spin 150* spin coater (right)

For solution processed devices all conditions were kept the same as in vacuum processed, except the emissive layer. First, MoO_3 were deposited on to clean ITO substrates, as a hole injection layer, in vacuum higher than $2 \cdot 10^{-6}$ mbar, then emissive layer was formed by spin coating toluene solutions containing different ratio of three emitters with the concentration of 2–3 mg/ml. Spin coating was carried out using *SPS Spin 150* spin coater which is in the same glovebox as vacuum deposition chamber. The 2000–3000 rpm speed, with acceleration of 50 rpm/s for 100 seconds were used for emissive layer. After spin-coating, the layers were dried at 70 °C for 30 min in inert atmosphere. Other functional layers such as TSPO1, TPBi, LiF and aluminium were vacuum deposited as usual.

Luminescence-current-voltage (LIV) characteristics were recorded utilizing certified photodiode *PH100-Si-HA-D0* together with the PC-based power and energy monitor *11S-LINK* (from *STANDA*) and *Keithley 2400C* source meter. EL spectra were taken by the *Avantes AvaSpec-2048XL* spectrometer. Device efficiencies were calculated using the luminance, current density, and EL spectra. The colour properties of OLEDs (CIE, CRI, CCT) were calculated by using a dedicated software which was officially provided by *The Global Lighting Associacion*[67].

3. Research results and discussion

In this work, two novel emitters from separate families of compounds were chosen to sutdy. Their structures are different but what they have in common is both of them are iridium (III) complexes and due to strong spin-orbit coupling iduced by heavy metal atom, both of them succesfully utilises triplets and exhibits phosphorescent emission. To make it easier to read, compounds were named after colour of emission: **Red** and **Orange**. Emitters were investigated by photophysical (steady-state and time-resolved spectroscopy), electrochemical (cyclic volammetry) and photoelctrical (electron photoemission spectroscopy) methods. The obtained results were used to develop structures for solution-processed white OLED with high quality electroluminescence featuring either high CRI, close to nature white CIE1931 coordinates of (0.33, 0.33), or human-eyes-friendly colour temperature of 3000 K.

3.1. Photophysical properties

In order to estimate the potential of **Red** and **Orange** emitters, UV-Vis and photoluminescence (PL) spectra of their dilute solutions and solid films were recorded (Fig. 20, Table 4). UV-Vis measurement shows that both compounds, in different media (toluene, THF and solid-state) demonstrated similar spectra and absorb UV and visible radiation up to region of green colour (500–550 nm). Low-energy absorption bands which corresponds to metal to ligand charge transfer (MLCT) were observed at 480–500 nm and 405–445 nm for **Red** and **Orange** emitters, respectively. The high energy peaks of both compounds at 290–370 nm region are originated from the ligand to ligand charge transfer (LLCT) and intraligand charge transfer (ILCT) which are related to the spin-allowed $^1\pi$–π^* transitions of iridium(III) complexes [68, 69].

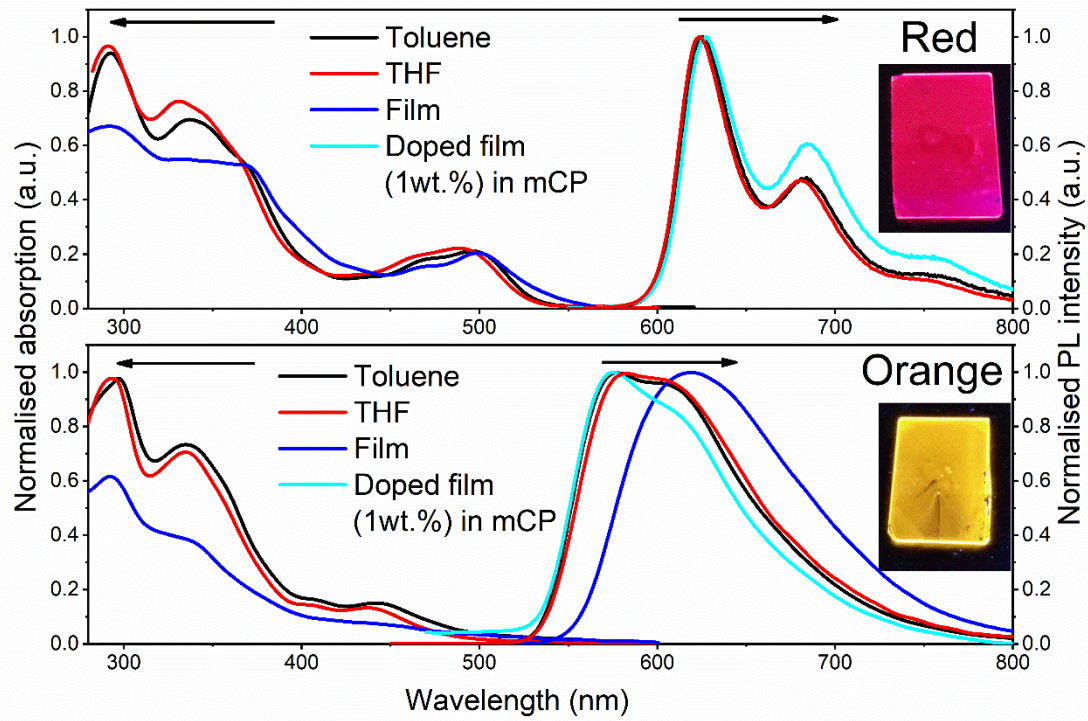

Fig. 20. Red and **Orange** emitters UV-Vis and PL spectra of dilute toluene and THF solutions, neat and doped 1 wt.% in mCP films. Pictures in right side are from doped thin film under UV excitation

Obviously, according to the name, **Red** compound in solutions demonstrated emission in deep red region with three distinct peaks at 625, 683 and 752 nm, while **Orange** compound exhibited structured PL spectra with 2 peaks at 578 and 603 nm which is at orange region. For both complexes, basically no solvatochromic effect were observed because in both solvents (toluene and THF) PL spectra was identical and no significant shift was detected. Since phosphorescence is very sensitive to oxygen (oxygen quenches the triplet states and blocks radiative relaxation), diluted solutions, as prepared, had very weak emission, especially with **Red** complex. When solutions were deoxygenated, both materials showed a large increase in emission intensity together with longer PL decay lifetime. Radiative emission of **Orange** increased 5.88 times, while **Red**, surprisingly, demonstrated even 26.3 times enhanced emission intensity. (Fig. 21 a). PL decay lifetimes τ_{max} reached 1.19μs for **Red** and 2.28 μs for **Orange** (Fig. 21 b). This observation proves that the absence of oxygen has strong contribution to efficient phosphorescence emission instead of non-radiative relaxation of excitons.

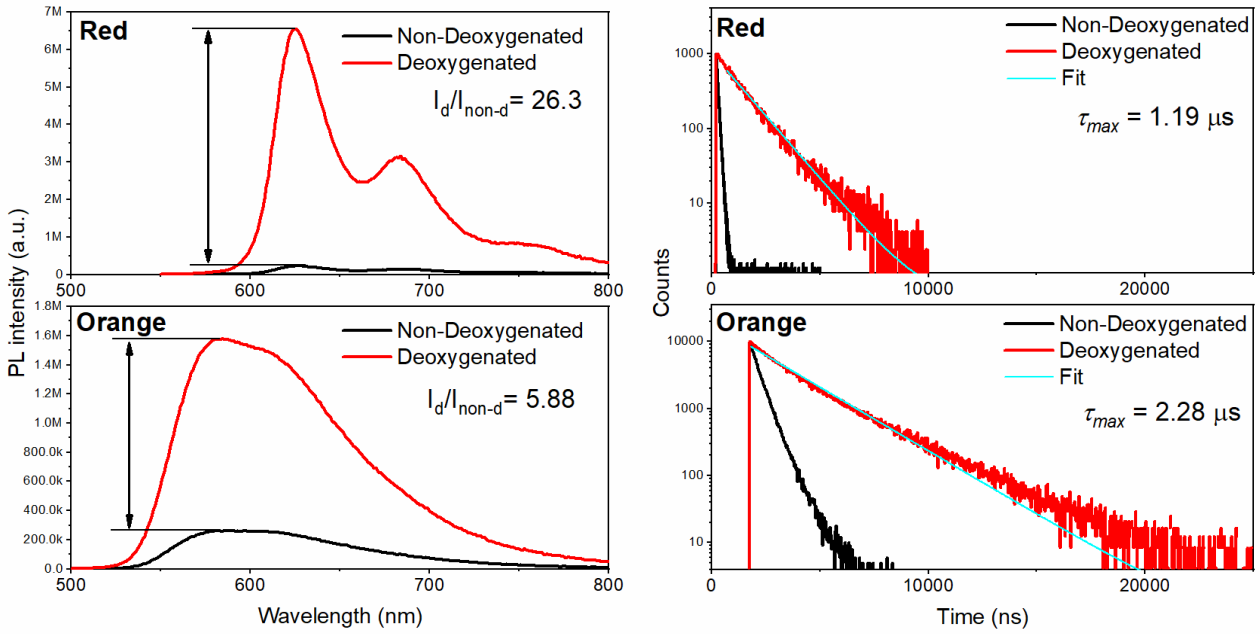

a) b)

Fig. 21. Deoxygenated and non-deoxygenated PL (a) and PL: decay (b) spectra of dilute toluene solutions (10^{-5} M) of **Red** and **Orange** complexes

Nondoped layers of both compounds, as usual for phosphorescent materials, had some difficulties. **Red** was practically non emissive (that's why there is no PL spectra of neat film in Figure 20), while **Orange** had weak, slightly redshifted emission with a maximum at 617 nm. Aggregation-induced quenching, non-effective TTA or just simple oxygen quenching could be the reason for low emission. However, things changed, when complexes were imbedded 1 wt.% into suitable matrix – mCP. For both materials, emission became intensive and had a similar shape of the spectra to toluene and THF solutions. Visual comparison of non-doped and doped film is at Figure 22.

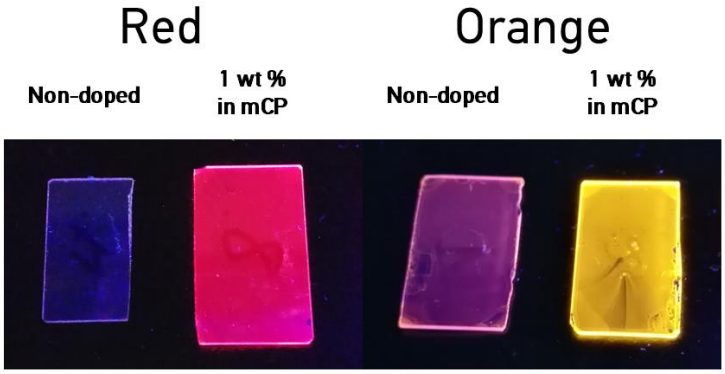

Fig. 22. Thin films of **Red** and **Orange** prepared by spin-coating on quartz substrates and excited by handheld UV lamp (ex. 350 nm). The non-doped film of **Red** looks blueish on photo due to lack of emission and UV rays reflects from substrate

Relatively high photoluminescence quantum yields (PLQY) value of 60% and 58% were recorded for deoxygenated toluene and THF solutions of **Orange**, respectively, while **Red** reached only 12% and 11% at the same conditions (Table 4). Neat films were not measured due to lack of emission but 1 wt.% doped films in mCP matrix were recorded and reached 25% and 31% for **Orange** and **Red** respectively. Need to address that measurements were carried out in air atmosphere, thus oxygen was able to interact with samples and quench emission. Most likely, if measured in inert atmosphere, the real PLQY could be higher. Overall, after photophysical investigation, iridium (III) complexes **Red** and **Orange** seems like promising phosphorescent compounds for electroluminescent devices if imbedded in host with appropriate energy levels. Therefore, further investigation of emitters can be implemented.

Table 4. The main photophysical characteristics

Emitter	Sample form	λ_{abs}, nm	λ_{PL}, nm	PLQY, %
Red	Deoxygenated toluene	292/336/496	625/683/752	12
	Deoxygenated THF	291/330/488	625/680/750	11
	Neat film	290/368/500	-	-
	1 wt % in mCP	-	625/684/752	31
Orange	Deoxygenated toluene	298/335/408/442	578/603	60
	Deoxygenated THF	293/335/405/438	582/603	58
	Neat film	292/332/443	620	4
	1 wt % in mCP	-	576/603	25

3.2. Electrochemical and Photoelectrical properties

The ionisation potentials (I_P) of compounds were estimated by cyclic voltammetry (CV) and photoelectron emission spectrocopy (PE) which results are presented in Figure 23 and Table 5. The I_P^{CV} values of compounds were estimated from the onset potentials of the first oxidation event after calibration of the measurements against ferrocene using formula (6) described in experimental methods section. Compound **Red** exhibited reversible, while **Orange** had non reversible electrochemical oxidation and calculated I_P^{CV} values were 5.07 and 5.26 eV, respectively. During CV

measurement, both compounds didn't show any sign of reduction process in the negative side of applied potential, this means electron affinity (E_A^{CV}) values couldn't be obtained by CV method. Need to highlight that I_P^{CV} and E_A^{CV} values corresponds to HOMO and LUMO of molecule, respectively.

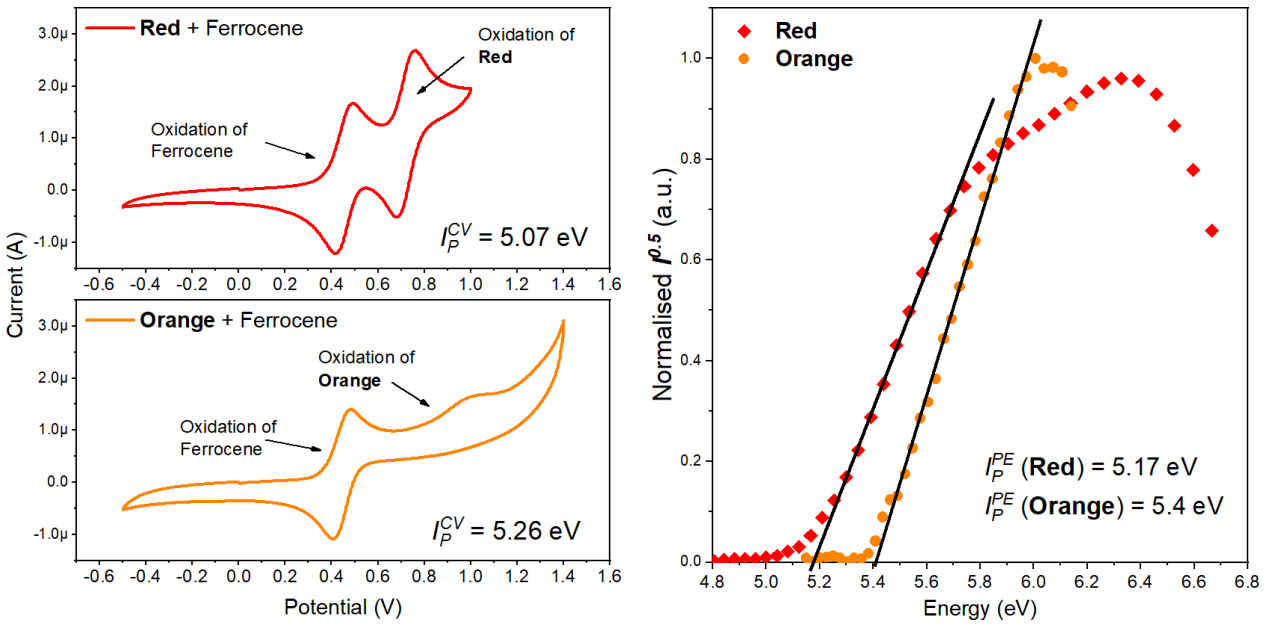

a) b)

Fig. 23. Cyclic voltammetry curve (a) and photoelectron emission spectra (b) of **Red** and **Orange** emitters

The I_P^{PE} of vacuum deposited layers were estimated from onset of photoelectron emission spectra, which were 5.17 eV for **Red** and 5.4 eV for **Orange** (Fig. 23 b). Results are in good agreement with trend of CV measurement – **Red** has approximately 0.2 eV lower value than **Orange**. As usual, I_P^{PE} values are little bit higher than I_P^{CV} because in solid state film, need to take into account additional binding energies [70]. Using formula (7), electron affinities of solid layers were calculated. Surprisingly, both compounds happened to have identical E_A^{PE} values of 2.87 eV. Optical band gap energy (E_g) of non-doped films were taken from onset of lowest energy absorption band using *Tauc* relation as described by *Swart et al* [66].

Table 5. Electrochemical and photoelectrical properties of investigated compounds

	I_P^{CV}, eV	I_P^{PE}, eV	E_A^{PE}, eV	E_g, eV
Red	5.07	5.17	2.87	2.3
Orange	5.26	5.4	2.87	2.53

3.3. Single-colour Phosphorescent OLEDs

In order to check the electroluminescent properties of the selected iridium (III) complexes, firstly they were tested in vacuum processed OLEDs, named **VR** and **VO** (**V** – vacuum deposited, **R** – including emitter **Red**, **O** – including emitter **Orange**). Structure were chosen considering measured ionisation potential and electron affinities values of solid-state samples: ITO/MoO_3(0.3 nm)/NPB(30 nm)/TCTA(8 nm)/mCP(8 nm)/5 wt.% of **Red** or **Orange**:mCP(20 nm)/TSPO1(8 nm)/TPBi(40 nm)/LiF:Al (Fig. 24). The hole-injection layer was deposited directly onto clean glass substrates with pre-patterned ITO anodes using MoO_3. To efficiently decrease the energy barrier (0.6 eV) between

hole-injection layer and the host, combination of two hole-transporting layers were prepared utilizing NPB and TCTA. Electron/exciton-blocking and hole/exciton-blocking layers were prepared using mCP and TSPO1, respectively. Layer of TPBi were deposited as electron-transporting and, finally, LiF was employed as an electron-injection layer. It was expected that using this structure, devices would have good charge balance, in other words, equal number of holes and electrons will meet and recombine at the emissive layer (EML).

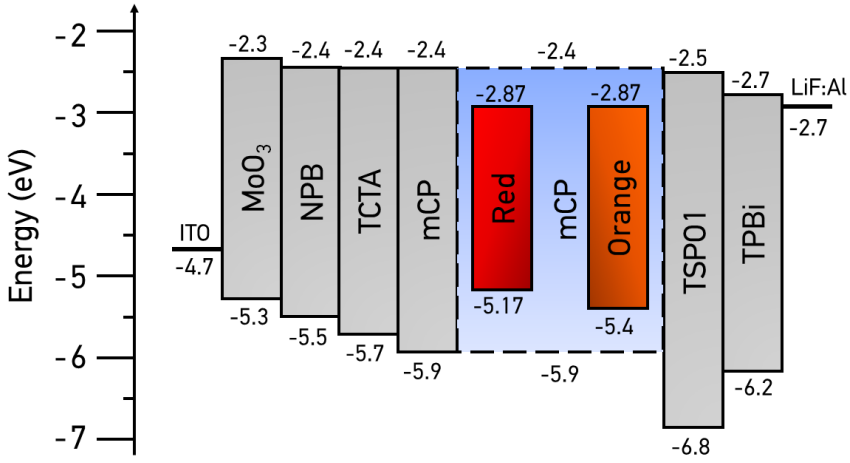

Fig. 24. Energy diagram of vacuum processed OLEDs.

Due to the good matching of HOMO and LUMO values of the chosen functional layers, the fabricated OLEDs demonstrated stable electroluminescence (EL) spectra at different applied voltages and those spectra were in very good agreement with PL spectra of doped solid films (Fig. 25 b). Device **VR1,** with emitter **Red**, discovered to have CIE 1931 coordinates of (0.69, 0.31), which surprisingly is deeper red than *National Television System Committee* (NTSC) red colour standard (0.67, 0.33) [71] and at the same time deeper than well-known and popular phosphorescent emitter bis(1-phenylisoquinoline)(acetylacetonate)iridium(III), better known in shorter name ($Ir(piq)_2(acac)$), which has a CIE of (0.68, 0.32) [72] (Fig. 25 a). On the other hand, device **VO1**, with emitter **Orange**, had CIE of (0.54, 0.46), which shows that deep orange colour could be used for warmer colour white OLEDs in combination with blue and green colour.

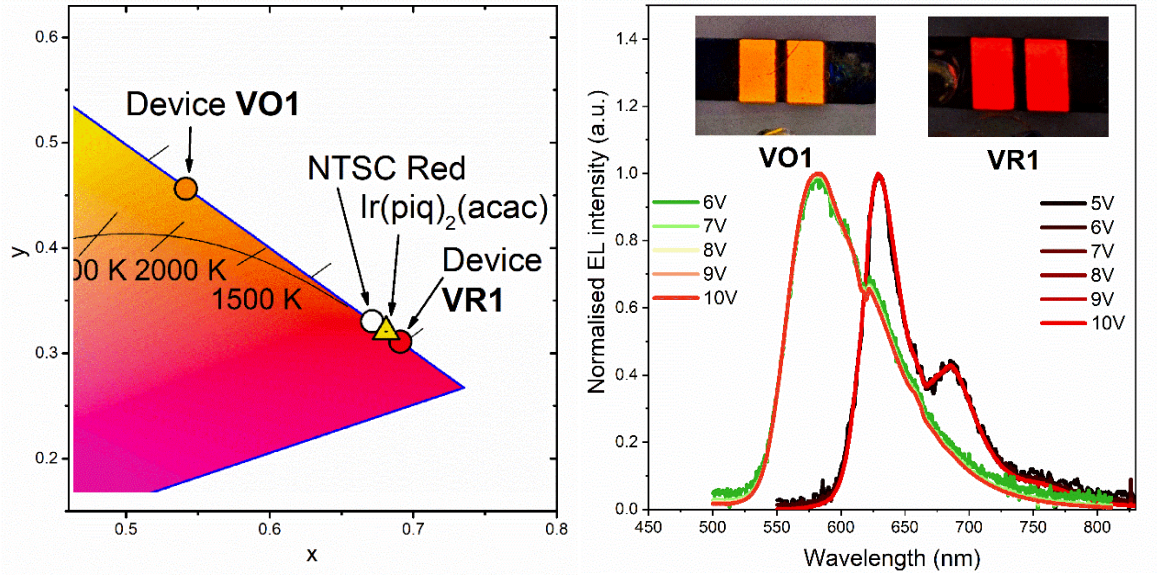

a) b)

Fig. 25. Zoomed-in red corner of CIE diagram with dots for devices **VO1**, **VR1** and NTSC red standard with $Ir(piq)_2(acac)$ (a) and EL spectra at different voltages of **VO1** and **VR1** devices with photos of real working pixels at the top (b)

Talking about *luminescence-current-voltage* (LIV) characteristics, phosphorescent OLED **VR1** exhibited maximum current, power efficacies (CE, PE) and external quantum efficiency (EQE) of 5.2 cd/A, 2.1 lm/W and 7.5%, respectively (Table 6). Turn on voltage (V_{ON}) was 5.6 V and maximum brightness achieved was 2250 cd/m^2. The EQE result of 7.5% is comparable to the first reported phosphorescent OLED, which was based on famous emitter $Ir(piq)_2(acac)$ and had 9.2% of EQE [72].

The device **VO1** performed very well and was characterised by V_{ON} of 5.0 V and brightness of 5200 cd/m^2. Even more, the maximum EQE of **VO1** was 17.5%, CE – 41.1 cd/A and PE – 25.6 lm/W (Table 6). The general trend of higher measured PLQYs of compound **Orange** could be the reason for much higher performance values of produced OLEDs by vacuum deposition. Brightness, current density and EQE characteristics are depicted at Figure 26. However, in this work, efficiencies are not only the only values that is important, colour properties are significant as well.

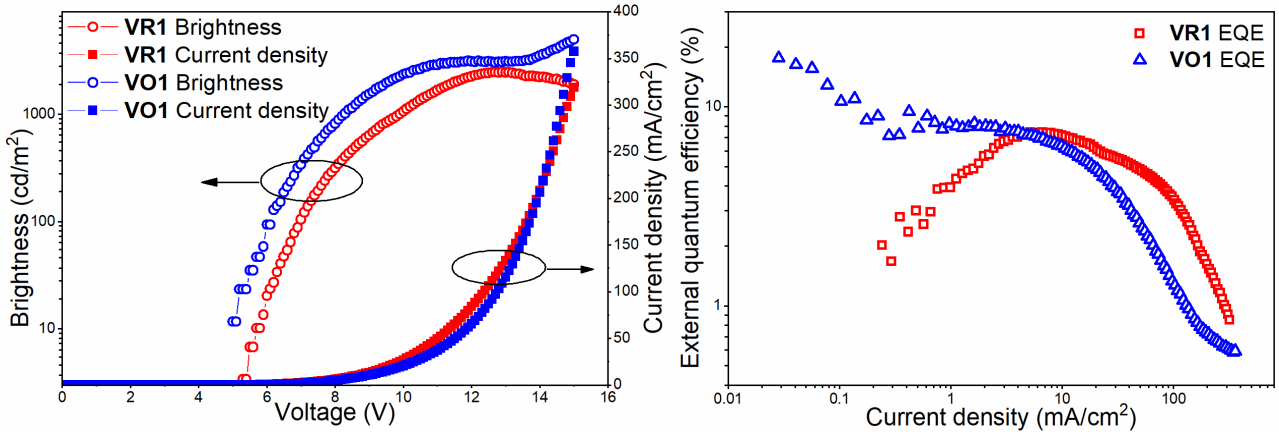

a) b)

Fig. 26. Brightness/current density versus voltage (a) and EQE values (b) of **VR1** and **VO1** devices.

3.4. White hybrid OLEDs

The main idea of this research, from the beginning, was to produce white OLEDs with decent colour characteristics. Until now, only two materials, which emits in red region, have been investigated in previous sections, so where is white colour here? The basic concept to produce white colour is the same as in nature, mix three main colours of red, green, blue (RGB) and if their intensities are close to equal, white colour will be observed. This means in order to get white, OLED needs to emit wide EL spectra, which covers full visible region.

One solution to this problem was to mix three emitters in one emissive layer and naively hope for the white colour, but immediately there was a first obstacle to overcome: it is impossible to deposit three organic materials at one time using our vacuum chamber equipment. Other popular OLED producing method, of which, at that time, I didn't had any experience, needed to be used – solution processing, where emissive layer is spin coated from prepared liquid solutions and following layers can be finished by usual vacuum deposition. Then, it was decided to use the strategy of, so called, hybrid OLEDs, where the emissive layer is a combination of emitters utilising different relaxation mechanisms: fluorescent blue, TADF green and, of course, phosphorescent **Red** and **Orange** emitters. And from this point, the biggest issue was to deal with countless number of choices: which blue and green emitters to choose? What part of ratio to use of each emitter? Which hole injection layer to deposit? Which solvent to use for spin coating? What concentration to use for solutions? And so on. Every small detail has an impact on emission behaviour, therefore at least a 9 series of 6 to 8 devices, utilising **Red** or **Orange** emitters, which each of them has 6 emitting pixels, were produced. This adds up to a total of 50 to 70 units produced. Some of them were only for testing the idea, some of them were repeated several times and some of them had wrong emission colour or just simply did not work. This means that lots of optimisation has been done and it is impossible to cover all of them in this work, so only the most important ones will be discussed below.

3.4.1. 1st series of hybrid OLEDs.

After some research, it was decided, that NPB could work as a blue emitter and at the same time as a host for TADF green and phosphorescent red materials due to suitable energy levels. Even though NPB is mostly used as hole transporting layers in OLEDs, but it has well balanced hole and electron charge mobilities, emission in deep-blue region and good solubility [73, 74, 75]. Those properties of NPB well matched our needs for a solution processable OLED. Additionally, for the green emitter, DACT-II was chosen due to its perfect TADF properties, small ΔE_{ST}, green colour and IQE reaching a full 100% [58].

Before making actual OLEDs, different solvents (chloroform, THF and toluene) with different concentrations were tested by spin coating on substrates and visually inspected for film quality. It was decided to use toluene solvent, as it is the least aggressive solvent (e.g. chloroform can cause some organic molecules to break down), it has lowest evaporation rate and formed the most uniform films on substrates.

First series of solution processed OLEDs are named **SRA** (**S** – solution processed, **R** – including emitter **Red**, **A** – first series). Their purpose was just to check the idea and try to find approximate ratio of each emitter to be mixed. It was known, that in case of high concentration of green or red emitters, emission from a blue host will not be observed. This means that in order to see emission of blue component, emissive layer must consist of at least ~95% of blue host, which is NPB, and only

~5% left for green and red components. So, considering this assumption, ultralow concentrations of DACT-II and **Red** had to be optimised in order to see white EL, therefore 99.8/0.1/0.1 wt.% (**SRA1**), 99/0.5/0.5 wt.% (**SRA2**) and 98/1/1 wt.% (**SRA3**) of NPB/DACT-II/**Red** were utilised respectively. The structure of devices were ITO/MoO_3(2 nm)/NPB:DACT-II:**Red**(30 nm)/TSPO1(8 nm)/TPBi(40 nm)/LiF:Al (Figure 28), in which the roles of additional layers were the same as those described in the previous section. Emissive layer was spin coated at 3000 rpm setting for 100 seconds from toluene solution of mixed emitters with 2 mg/ml concentration.

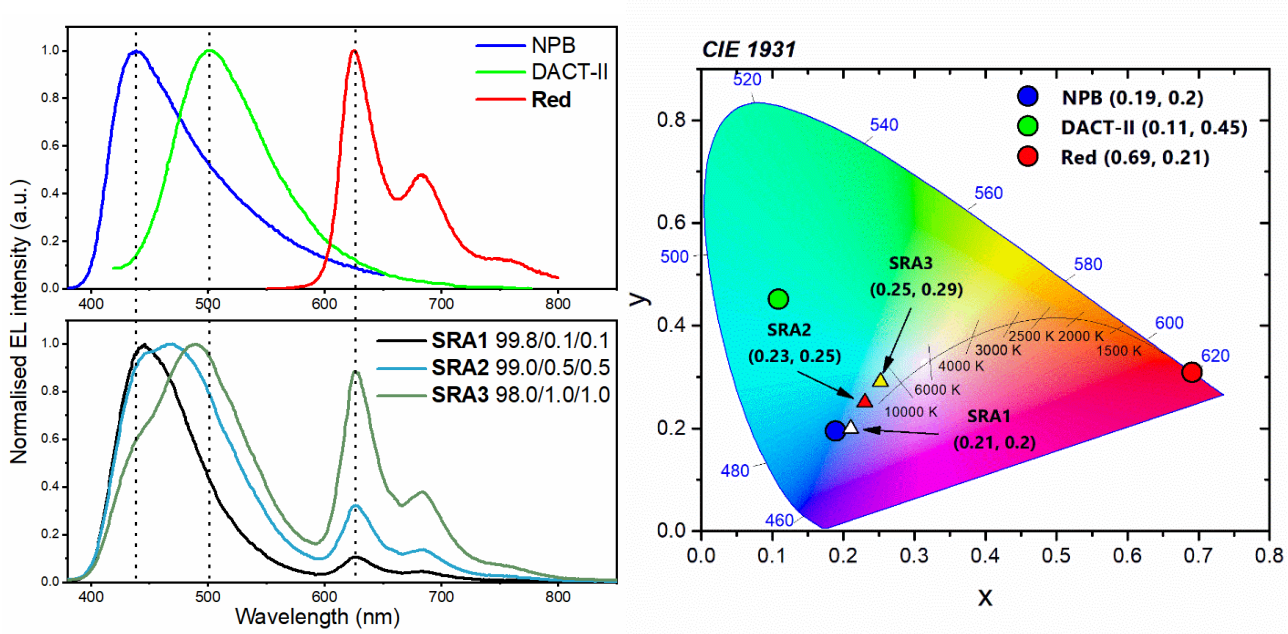

a) b)

Fig. 27. EL emission spectra of NBP, DACT-II and **Red** at the top (a), EL emission spectra at 9V of **SRA1**, **SRA2** and **SRA3** OLEDs at the bottom (a) and CIE 1931 plot with device coordinates plotted.

OLEDs were working but as could be expected, colour was not yet perfectly white from the first try. EL spectra of devices, compared to separate spectra of each emitter, together with CIE diagram can be seen in Figure 27. Device **SRA1**, with ultralow concentration of DACT-II and **Red** (0.1/0.1 wt.%), had mostly blue spectra with just a hint of red, CIE coordinates were calculated to be (0.21, 0.2) which is really close to pure NPB CIE of (0.19, 0.2). Following device **SRA2**, with 0.5/0.5 wt.% concentration of DACT-II/**Red** clearly had some shoulder of green emission and stronger component of red but overall, it was still bluish colour with a CIE of (0.23, 0.25). Third, **SRA3**, with highest concentration of 1/1 wt.% (DACT-II/**Red**) was closest to white colour with obviously strong components of green, red and a shoulder of blue but CIE of (0.25, 0.29) was still far from ideal (0.33, 0.33). Calculated colour rendering index (CRI) and correlated colour temperature (CCT) for **SRA3** was 63 and 10467 K, respectively, which was far from our vision. Also, the spectra itself was not uniform, it had wide gap of low emission in region of 520-620 nm, which meant that more redshifted green emitter must be used in order to get equal coverage of visible region and good quality white light. CRI and CCT values could not be calculated for **SRA1** and **SRA2** because it was not enough white, or in other words, it was too far away from ideal black body radiator (Planckian locus line on CIE diagram), which is used for calculations.

3.4.2. 2nd series of hybrid OLEDs

For the second series of white solution processed OLEDs (**SRB**), green emitter needed to be changed to more red-shifted one. The DAcIPN [60] was chosen for this task due to good TADF properties and emission peak at 521 nm, compared to 500 nm of previously used DACT-II, which should provide better coverage of visible spectra. The device structure was kept the same: ITO/MoO_3(2 nm)/NPB:DAcIPN:**Red**(40 nm)/TSPO1(8 nm)/TPBi(40 nm)/LiF:Al (Figure 28). Only changes were increased concentration of final toluene solution of emitting layer from 2 mg/ml to 3 mg/ml and decreased spin coater speed from 3000 rpm to 2000 rpm. This helped to get little bit thicker emissive layer of 40 nm vs. 30 nm previously.

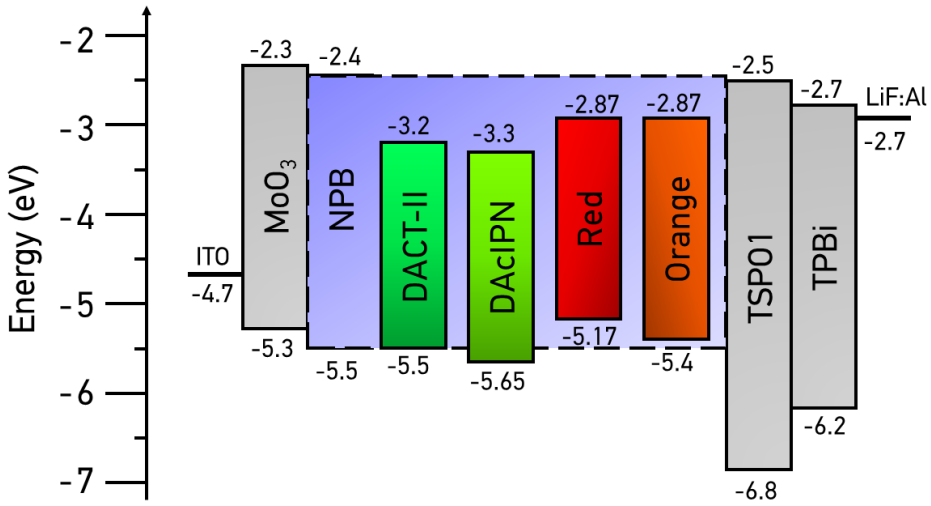

Fig. 28. Energy diagram of solution processed white OLEDs (**SRA**, **SRB, SOC**).

For the **SRB** series, the decision was made to keep constant amount of green emitter (2 wt.%) and only change the ultralow part of **Red** with the aim of calibrating the intensity of red colour component in EL spectra. Hence four devices were produced: 97.8/2/0.2 wt.% (**SRB1**), 97.6/2/0.4 wt.% (**SRB2**), 97.4/2/0.6 wt.% (**SRB3**) and 97.2/2/0.8 wt.% (**SRB4**) of NPB/DAcIPN/**Red**, respectively.

The EL spectra of **SRB** series OLEDs was characterised by real white colour with a CIE coordinates close to natural white (0.33, 0.33), calculated CRI reached maximum of 85 and CCT was ranging from 2780 to 6140 K (Table 6, Fig. 29). The OLED **SRB3** with CIE coordinates of (0.34, 0.35) (Fig. 29 b) was closest to natural white CIE of (0.33, 0.33). Looking at the EL spectra (Fig. 29 a) it is obvious that changing the green TADF emitter paid of well. RGB components of **SRB** series were distributed more evenly across visible region, without any significant gaps. Also, the DAcIPN CIE coordinates of (0.35, 0.57) helped to form bigger imaginary triangle between all three RGB components (Fig. 29 b), which means that more colours could be reproduced by using different ratios of each component, compared to the **SRA** series. Device **SRB1**, with the lowest amount of emitter **Red** (0.2 wt.%) demonstrated the most uniform spectra, therefore it reached highest CRI value of 85. By increasing the part of **Red**, spectra gradually became dominated by red component which means, that colour would not be rendered as accurately. Nonetheless, it is considered as good achievement because all 4 devices were close to the Planckian locus (Fig. 29 b), which represents ideal black body radiator.

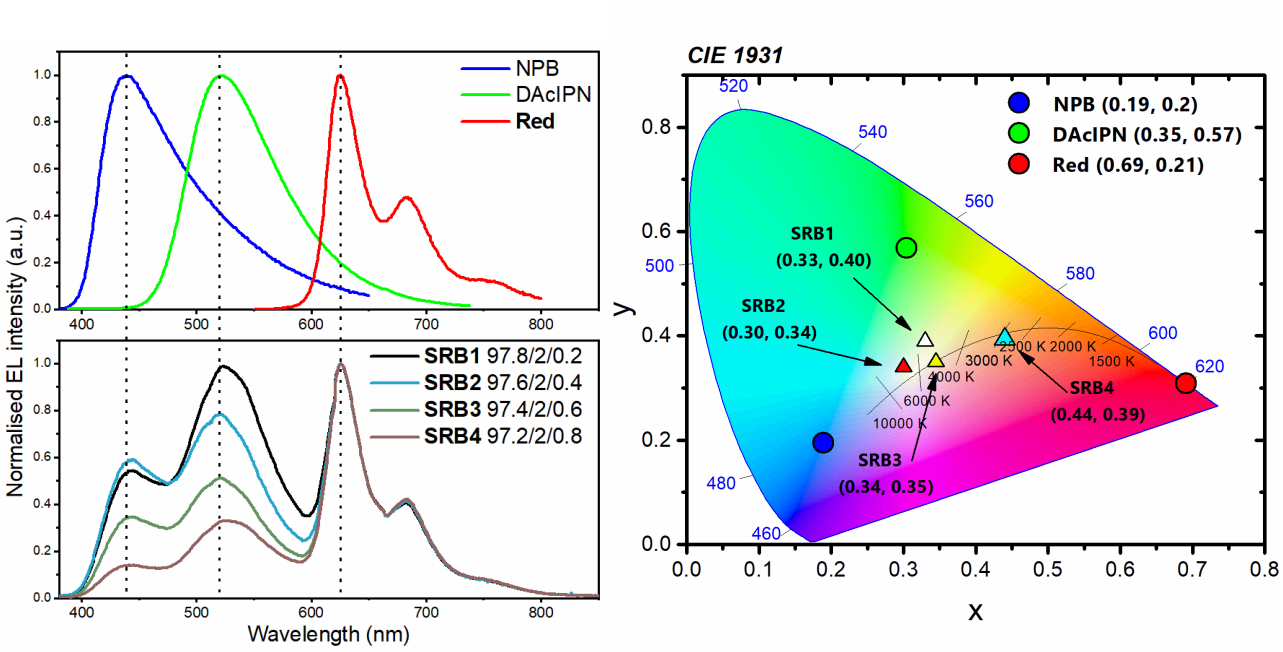

a) b)

Fig. 29. EL emission spectra of NBP, DAcIPN and **Red** at the top (a), EL emission spectra at 6V of **SRB1**, **SRB2**, **SRB3** and **SRB4** OLEDs at the bottom (a) and CIE 1931 plot with device coordinates plotted.

The **SRB** series devices showed relatively low V_{ON} in range of 3.6–4.3 V with high brightness exceeding 10 000 cd/m^2 (Fig. 30, Table 6). The highest maximum power, current efficacies and EQE of 5.1 lm/W, 8.7 cd/A and 6.3%, respectively, were achieved by **SRB4** OLED with greatest concentration of **Red** emitter (0.8 wt.%) (Table 6). It is a good example that even ultralow concentration of triplet harvesting material (TADF and phosphorescence) can help to overcome theoretical EQE limit of 5% for fluorescence-based devices.

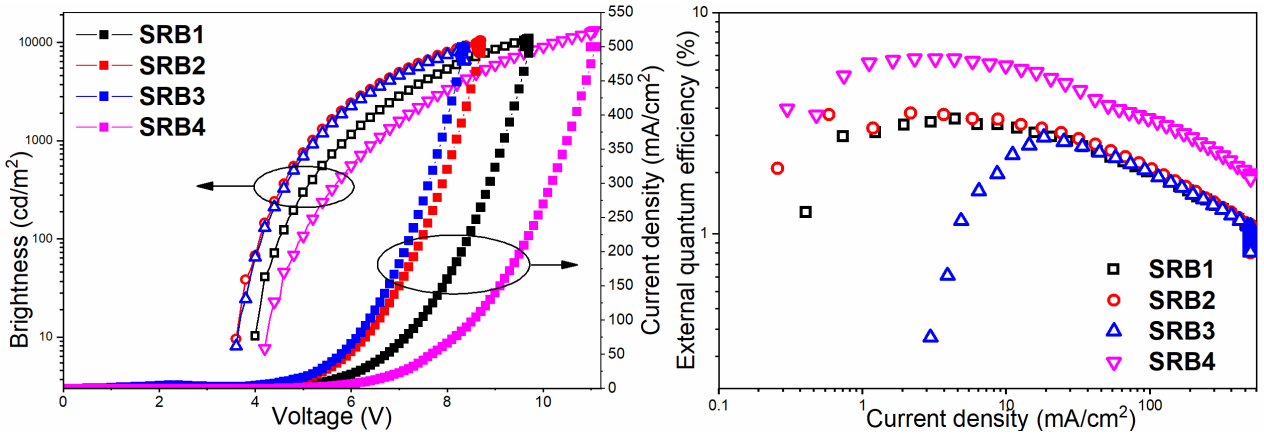

a) b)

Fig. 30. Brightness/current density versus voltage (a) and EQE values (b) of **SRB** series devices.

3.4.3. 3rd series of hybrid OLEDs

With the **Red** emitter being thoroughly investigated and proven to be working in setup of white OLEDs, time comes to test what an **Orange** iridium (III) complex is capable of. Already having some experience of colour tuning in previous devices, since it was reliably working, the decision was made to use the same blue and green components and keep the device structure as in the second **SRB** series: ITO/MoO_3(2 nm)/NPB:DAcIPN:**Orange**(40 nm)/TSPO1(8 nm)/TPBi(40 nm)/LiF:Al (Fig. 28). The emissive layer formation method was also kept in the same manner: final emissive layer solution concentration of 3 mg/ml and spin coating at 2000 rpm speed for 100 seconds, which gave the resulting thickness of 40 nm. For the third series of OLEDs (**SOC**) the amount of DAcIPN was also kept the same (2 wt.%) and only part of **Orange** was changed with increments of 0.5 wt.% in order to calibrate emission. Therefore, three devices were produced: 97.5/2/0.5 wt.% (**SOC1**), 97/2/1 wt.% (**SOC2**) and 96.5/2/1.5wt.% (**SOC3**) of NPB/DAcIPN/**Orange**, respectively.

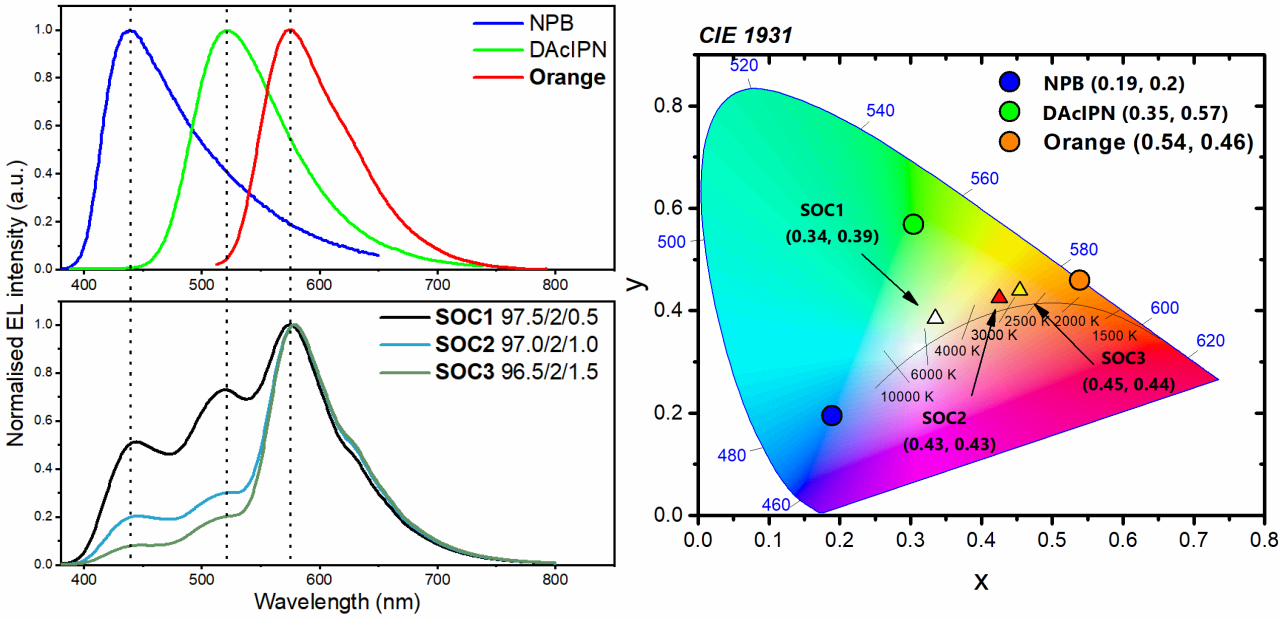

a) b)

Fig. 31. EL emission spectra of NBP, DAcIPN and **Orange** at the top (a), EL emission spectra at 6V of **SOC1**, **SOC2** and **SOC3** OLEDs at the bottom (a) and CIE 1931 plot with device coordinates plotted.

The EL spectra of **SOC** series hybrid OLEDs were characterised by three well-seen emission bands at 440, 520, and 578 nm, which are in very good agreement with the corresponding EL spectra of devices based on emitters NPB, DAcIPN and **Orange** (Fig. 31, Table 6). By gradually increasing concentration of **Orange**, intensities of green and blue components relatively decrease, forcing spectra shift to warmer colour emission. Highest CRI value of 72 was calculated for device **SOC1** with lowest concentration (0.5 wt.%) of **Orange**. The **SOC2** and **SOC3** OLEDs, with higher concentration of **Orange**, both demonstrated human eyes friendly warm colour emission with calculated CCT of 3070 K and 2910 K, respectively. The OLED **SOC1** with CIE coordinates of (0.34, 0.39) (Fig. 31 b) was closest to natural white CIE of (0.33, 0.33). Overall, **SOC** series presented EL spectra with a tendency of warmer white colour tone, which proves that emitter **Orange** can be successfully used for human eyes friendly white colour OLEDs.

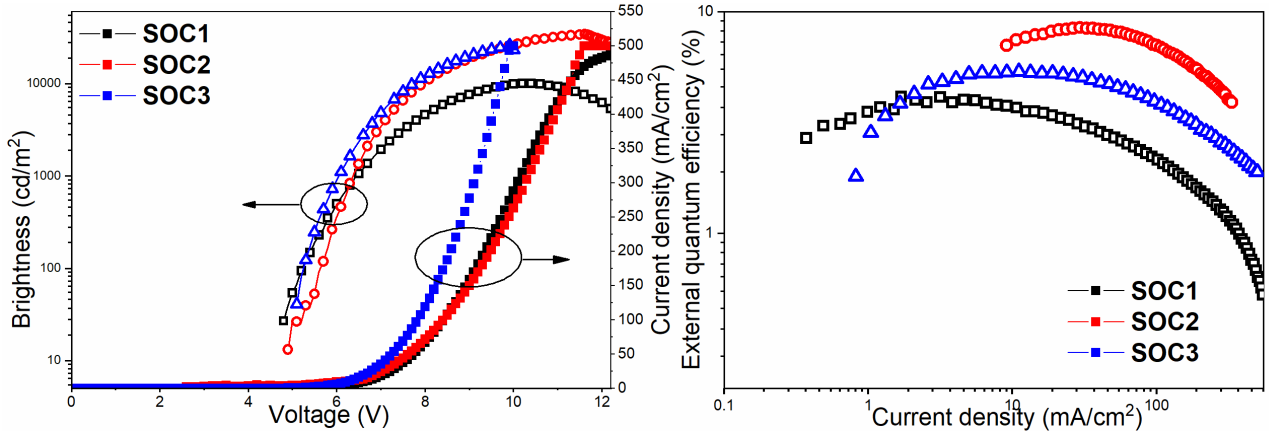

a) b)

Fig. 32. Brightness/current density versus voltage (a) and EQE values (b) of **SRB** series devices.

The **SOC** series devices demonstrated V_{ON} in range of 4.8–5.1 V. Devices **SOC2** and **SOC3** exhibited extremely high brightness exceeding 20 000 cd/m^2, when operating at higher than 9 V voltages (Fig. 32, Table 6). The highest maximum power, current efficacies and EQE of 9.5 lm/W, 23.1 cd/A and 8.7%, respectively, were achieved by **SOC2** OLED with concentration of 1 wt.% of **Orange** emitter (Table 6). Well balanced energetical device structure and perfectly formed functional layers could be the reason of high efficiency and brightness values for **SOC2** OLED.

Table 6. Characteristics of OLEDs

Device	Emissive layer composition[a]	V_{ON}, V	Max. brightness, cd/m^2	CE_{max}, cd/A	PE_{max}, lm/W	EQE_{max}, %	CIE 1931 (x, y)	CRI	CCT, K
Vacuum processed OLEDs with structure *ITO/MoO_3/NPB/TCTA/mCP/emitter 5%:mCP/TSPO1/TPBi/LiF:Al*									
VR1	**Red**	5.6	2250	5.2	2.1	7.5	(0.69, 0.31)	-	-
VO1	**Orange**	5.0	5200	41.1	25.6	17.5	(0.54, 0.46)	-	-
Solution processed OLEDs with structure *ITO/MoO_3/NPB(**X** wt.%):DACT-II(**Y** wt.%):**Red**(**Z** wt.%)/TSPO1/TPBi/LiF:Al*									
SRA1	99.8/0.1/0.1	3.8	6100	1.9	1.2	1.6	(0.21, 0.2)	-	-
SRA2	99/0.5/0.5	4.2	6900	2.0	1.3	1.7	(0.23, 0.25)	-	-
SRA3	98/1/1	3.9	8900	2.9	1.9	1.9	(0.25, 0.29)	63	10470
Solution processed OLEDs with structure *ITO/MoO_3/NPB(**X** wt.%):DAcIPN(**Y** wt.%):**Red**(**Z** wt.%)/TSPO1/TPBi/LiF:Al*									
SRB1	97.8/2/0.2	4	11000	6.7	4.3	3.3	(0.33, 0.40)	85	4930
SRB2	97.6/2/0.4	3.7	10400	6.4	4.3	3.4	(0.30, 0.34)	77	6140
SRB3	97.4/2/0.6	3.7	8800	4.4	2.7	2.7	(0.34, 0.35)	61	4320
SRB4	97.2/2/0.8	4.3	12300	8.7	5.1	6.3	(0.44, 0.39)	59	2780
Solution processed OLEDs with structure *ITO/MoO_3/NPB(**X** wt.%):DAcIPN(**Y** wt.%):**Orange**(**Z** wt.%)/TSPO1/TPBi/LiF:Al*									
SOC1	97.5/2/0.5	4.8	10200	10.5	6.2	4.2	(0.34, 0.39)	72	4930
SOC2	97/2/1	4.9	33800	23.1	9.5	8.7	(0.43, 0.43)	58	3070
SOC3	96.5/2/1.5	5.1	25850	15.0	7.8	5.5	(0.45, 0.44)	55	2910

[a] emissive layer composition for solution processed devices are denoted as percentage part of each of three colour components X/Y/Z wt.%

Interestingly, the colour properties of different series devices correlate perfectly in between, even though different low energy emitter were used. For example, **SRB1** and **SOC1** displayed identical CCT value of 4930 K and were really close to each other in terms of CIE coordinates: (0.33, 0.40) and (0.34, 0.39), respectively, and at the same time very close to perfect natural white of (0.33, 0.33) (Fig. 33). Calculated CRI values were different: 72 for **SOC1** and significantly higher 85 for **SRB1** OLED. This is obviously due to deeper red colour emitter **Red** used in **SRB** series, which helps to cover a greater part of visible region, thus corresponding with a better rendering of colours.

Also, three devices were produced (**SRB4**, **SOC2**, **SOC3**), which exhibited human eyes friendly, warm colour emission with CCT in range of 2780–3070 K. This range perfectly covers the temperature range of classic incandescence bulb (2700–3000 K), which continues to be used as a benchmark when discussing white light sources. All three devices were close to the Planckian locus and really near to each other with CIE coordinates of (0.44, 0.39), (0.43, 0.43) and (0.45, 0.44) for **SRB4**, **SOC2** and **SOC3**, respectively (Fig. 33).

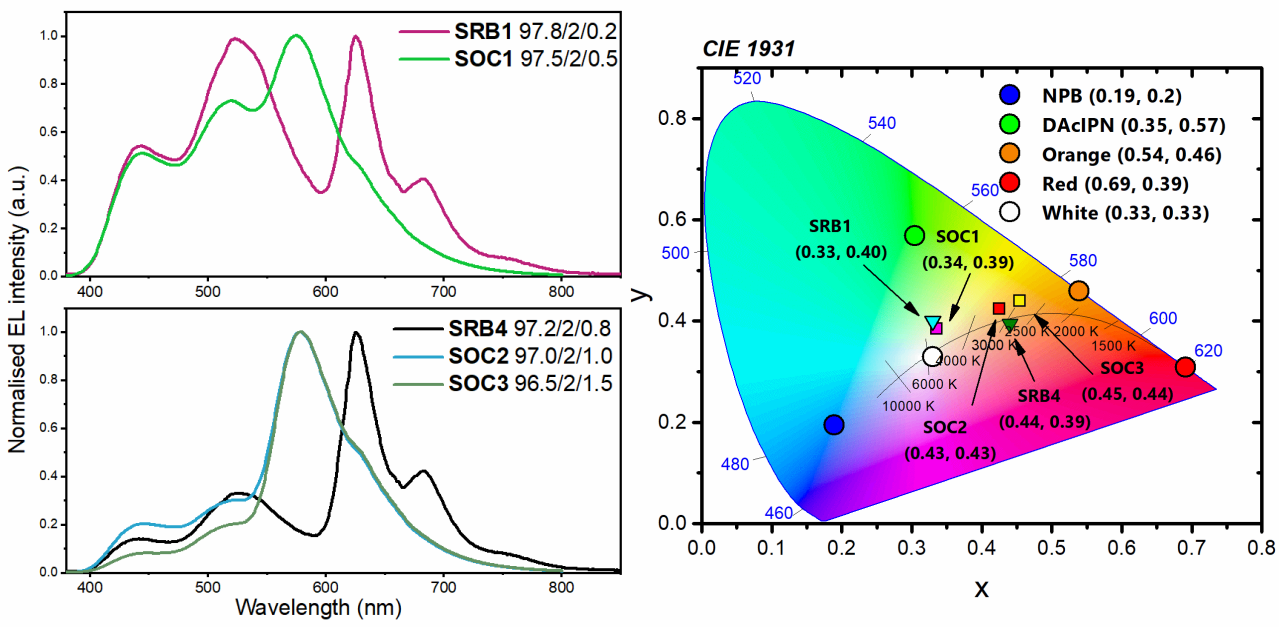

a) b)

Fig. 33. EL emission spectra of **SRB1** and **SOC1** OLEDs at the top (a), and **SRB4**, **SOC2** and **SOC3** OLEDs at the bottom (a) and CIE 1931 plot with device coordinates plotted.

Conclusions

1. Newly synthesised iridium (III) complexes **Red** and **Orange** were investigated by photophysical, electrochemical and photoelectrical techniques. The analysed compound **Orange** demonstrated emission with two peaks at 578 and 603 nm, while **Red** was more red-shifted and had three distinct peaks at 625, 683 and 752 nm in dilute solutions. Both compounds exhibited enhanced emission intensity in deoxygenated toluene solutions, 5.88 times for **Orange** and impressive 26.3 times for **Red**. Such emission increasement, combined with long lived decays of photoluminescence, proved that origin of emission is phosphorescence. Moreover, in deoxygenated toluene **Red** exhibited 12%, while **Orange** managed to reach 60% of photoluminescence quantum yield.
2. Vacuum processed prototype OLEDs were produced in order to test the electroluminescent properties of both selected compounds, which was in good agreement with a photoluminescence spectra. Device **VR1,** with emitter **Red**, reached 7.5%, while device **VO1**, with emitter **Orange**, was more efficient and showed 17.5% of external quantum efficiency. **SRA** series of solution processed prototype OLEDs were fabricated using combination of different ratios of NPB (blue), DACT-II (green) and **Red** emitter in emissive layer which proved the concept of colour tunability by utilising strategy of hybrid emissive layer. Electroluminescence was observed at a blue region. Conclusions were made to choose different green emitter with slightly red-shifted photoluminescence peak
3. Optimised solution processed OLEDs were characterised by high quality white electroluminescence. Device **SRB3** (97.4% NPB, 2% DAcIPN, 0.6% **Red**) with a CIE coordinates of (0.34, 0.35) was the closest to a natural white CIE of (0.33, 0.33). Highest colour rendering index value of 85 was reached by OLED **SRB1** (97.8% NPB, 2% DAcIPN, 0.2% **Red**). Furthermore, three devices **SRB4** (97.2% NPB, 2% DAcIPN, 0.8% **Red**), **SOC2** (97% NPB, 2% DAcIPN, 1% **Orange**) and **SOC3** (96.5% NPB, 2% DAcIPN, 1.5% **Orange**) were characterised by a warm colour, human eyes friendly white colour emission with a correlated colour temperature of 2780, 2910 and 3070 K, respectively.

List of references

1. *Energy Savings Forecast of Solid-State Lighting in General Illumination Applications*, 2019a. [online]. Washington, DC. [Accessed 26 April 2020]. Available from: https://www.energy.gov/sites/prod/files/2020/02/f72/2019_ssl-energy-savings-forecast.pdf
2. REINEKE, Sebastian, THOMSCHKE, Michael, LÜSSEM, Björn and LEO, Karl, 2013b. White organic light-emitting diodes: Status and perspective. *Reviews of Modern Physics* [online]. 30 July 2013. Vol. 85, no. 3, p. 1245–1293. DOI 10.1103/RevModPhys.85.1245. Available from: https://link.aps.org/doi/10.1103/RevModPhys.85.1245
3. YAM, Vivian W.W., 2010c. *WOLEDs and Organic Photovoltaics* [online]. Berlin, Heidelberg: Springer Berlin Heidelberg. [Accessed 8 April 2020]. Green Energy and Technology. ISBN 978-3-642-14934-4. Available from: http://link.springer.com/10.1007/978-3-642-14935-1
4. FALCHI, Fabio, CINZANO, Pierantonio, ELVIDGE, Christopher D., KEITH, David M. and HAIM, Abraham, 2011d. Limiting the impact of light pollution on human health, environment and stellar visibility. *Journal of Environmental Management* [online]. 1 October 2011. Vol. 92, no. 10, p. 2714–2722. [Accessed 26 April 2020]. DOI 10.1016/j.jenvman.2011.06.029. Available from: https://linkinghub.elsevier.com/retrieve/pii/S030147971100226X
5. ZHAO, Zhi-Chun, ZHOU, Ying, TAN, Gang and LI, Juan, 2018e. Research progress about the effect and prevention of blue light on eyes. *International Journal of Ophthalmology* [online]. 18 December 2018. Vol. 11, no. 12, p. 1999–2003. [Accessed 26 April 2020]. DOI 10.18240/ijo.2018.12.20. Available from: http://www.ijo.cn/gjyken/ch/reader/view_abstract.aspx?file_no=20181220&flag=1
6. SCHEUERMAIER, Karine, MÜNCH, Mirjam, RONDA, Joseph M. and DUFFY, Jeanne F., 2018f. Improved cognitive morning performance in healthy older adults following blue-enriched light exposure on the previous evening. *Behavioural Brain Research* [online]. 1 August 2018. Vol. 348, p. 267–275. [Accessed 26 April 2020]. DOI 10.1016/j.bbr.2018.04.021. Available from: https://linkinghub.elsevier.com/retrieve/pii/S0166432817315358
7. GABEL, Virginie, REICHERT, Carolin F., MAIRE, Micheline, SCHMIDT, Christina, SCHLANGEN, Luc J. M., KOLODYAZHNIY, Vitaliy, GARBAZZA, Corrado, CAJOCHEN, Christian and VIOLA, Antoine U., 2017g. Differential impact in young and older individuals of blue-enriched white light on circadian physiology and alertness during sustained wakefulness. *Scientific Reports* [online]. 8 December 2017. Vol. 7, no. 1, p. 7620. [Accessed 26 April 2020]. DOI 10.1038/s41598-017-07060-8. Available from: http://www.nature.com/articles/s41598-017-07060-8
8. MÜNCH, Mirjam, NOWOZIN, Claudia, REGENTE, Johannes, BES, Frederik, DE ZEEUW, Jan, HÄDEL, Sven, WAHNSCHAFFE, Amely and KUNZ, Dieter, 2016h. Blue-Enriched Morning Light as a Countermeasure to Light at the Wrong Time: Effects on Cognition, Sleepiness, Sleep, and Circadian Phase. *Neuropsychobiology* [online]. 1 July 2016. Vol. 74, no. 4, p. 207–218. [Accessed 26 April 2020]. DOI 10.1159/000477093. Available from: https://www.karger.com/Article/FullText/477093
9. HELLERICH, Emily S., 2013i. *Studies of solution-processed organic light-emitting diodes and their materials* [online]. Ames: Iowa State University, Digital Repository. Available from: https://lib.dr.iastate.edu/etd/13552/
10. SANTOS, Lucas Fugikawa and GOZZI, Giovani, 2016j. Electrical Properties of Polymer Light-Emitting Devices. In: *Conducting Polymers* [online]. InTech. Available from:

http://www.intechopen.com/books/conducting-polymers/electrical-properties-of-polymer-light-emitting-devices

11. MURAWSKI, Caroline, 2015k. *Efficiency Roll-Off in Organic Light-Emitting Diodes* [online]. Technical University of Dresden. [Accessed 26 March 2020]. Available from: https://nbn-resolving.org/urn:nbn:de:bsz:14-qucosa-179235
12. MANNA, Eeshita, 2017l. *Enhanced light out-coupling of organic light emitting devices (OLEDs) using novel plastic substrates and improved performance of OLED-based photoluminescence sensing platforme* [online]. Ames: Iowa State University, Digital Repository. Available from: https://lib.dr.iastate.edu/etd/15360/
13. KROTKUS, Simonas, 2016m. *Advances in Organic Displays and Lighting* [online]. Technical University of Dresden. [Accessed 26 March 2020]. Available from: https://tud.qucosa.de/landing-page/?tx_dlf[id]=https%3A%2F%2Ftud.qucosa.de%2Fapi%2Fqucosa%253A30995%2Fmets
14. SHINAR, Joseph (ed.), 2004n. *Organic Light-Emitting Devices* [online]. New York, NY: Springer New York. ISBN 978-1-4419-2960-0. Available from: http://link.springer.com/10.1007/978-0-387-21720-8
15. REINEKE, Sebastian, 2009o. *Controlling Excitons : Concepts for Phosphorescent Organic LEDs at High Brightness Sebastian Reineke* [online]. Technical University of Dresden. [Accessed 26 March 2020]. Available from: https://tud.qucosa.de/landing-page/?tx_dlf[id]=https%3A%2F%2Ftud.qucosa.de%2Fapi%2Fqucosa%253A25358%2Fmets
16. HOFMANN, Simone, 2012p. *Exciton Dynamics in White Organic Light-Emitting Diodes comprising Triplet Harvesting* [online]. Technical University of Dresden. [Accessed 26 March 2020]. Available from: http://nbn-resolving.de/urn:nbn:de:bsz:14-qucosa-117447
17. KAVOKIN, Alexey, BAUMBERG, Jeremy J., MALPUECH, Guillaume and LAUSSY, Fabrice P., 2007q. *Microcavities*. New York, NY: Oxford University Press Inc. ISBN 0198782993.
18. BRÜTTING, Wolfgang, 2005r. *Physics of Organic Semiconductors* [online]. Wiley. [Accessed 29 March 2020]. ISBN 9783527405503. Available from: https://onlinelibrary.wiley.com/doi/book/10.1002/3527606637
19. KÖHLER, A. and BÄSSLER, H., 2009s. Triplet states in organic semiconductors. *Materials Science and Engineering R: Reports*. 30 November 2009. Vol. 66, no. 4–6, p. 71–109. DOI 10.1016/j.mser.2009.09.001.
20. ATKINS, Peter and FRIEDMAN, Ronald, 2005t. *Molecular Quantum Mechanics Fourth Edition*. 4th. Oxford University Press Inc. ISBN 0199274983.
21. VALEUR, Bernard, 2009u. Molecular Fluorescence. In: *digital Encyclopedia of Applied Physics* [online]. Weinheim, Germany: Wiley-VCH Verlag GmbH & Co. KGaA. p. 477–531. [Accessed 29 March 2020]. Available from: http://doi.wiley.com/10.1002/3527600434.eap684
22. VALEUR, Bernard, 2001v. *Molecular Fluorescence: Principles and Applications* [online]. ISBN 352729919X. Available from: http://www.citeulike.org/group/2000/article/2395562
23. DOS-SANTOS, PALOMA, LAYS, 2018w. *The Study of Thermally Activated Delayed Fluorescence Mechanism in Mono and Bimolecular Systems* [online]. Durham University. [Accessed 27 March 2020]. Available from: http://etheses.dur.ac.uk/12840/
24. KASHA, Michael, 1950x. *Characterization of electronic transitions in complex molecules*. 1 January 1950. The Royal Society of Chemistry.

25. ENDO, Ayataka, OGASAWARA, Mai, TAKAHASHI, Atsushi, YOKOYAMA, Daisuke, KATO, Yoshimine and ADACHI, Chihaya, 2009y. Thermally Activated Delayed Fluorescence from Sn4+-Porphyrin Complexes and Their Application to Organic Light Emitting Diodes - A Novel Mechanism for Electroluminescence. *Advanced Materials* [online]. 18 December 2009. Vol. 21, no. 47, p. 4802–4806. [Accessed 1 April 2020]. DOI 10.1002/adma.200900983. Available from: http://doi.wiley.com/10.1002/adma.200900983
26. ENDO, Ayataka, SATO, Keigo, YOSHIMURA, Kazuaki, KAI, Takahiro, KAWADA, Atsushi, MIYAZAKI, Hiroshi and ADACHI, Chihaya, 2011z. Efficient up-conversion of triplet excitons into a singlet state and its application for organic light emitting diodes. *Applied Physics Letters*. 21 February 2011. Vol. 98, no. 8. DOI 10.1063/1.3558906.
27. UOYAMA, Hiroki, GOUSHI, Kenichi, SHIZU, Katsuyuki, NOMURA, Hiroko and ADACHI, Chihaya, 2012aa. Highly efficient organic light-emitting diodes from delayed fluorescence. *Nature*. 2012. Vol. 492. DOI 10.1038/nature11687.
28. ADACHI, Chihaya, BALDO, Marc A., THOMPSON, Mark E. and FORREST, Stephen R., 2001ab. Nearly 100% internal phosphorescence efficiency in an organic light emitting device. *Journal of Applied Physics* [online]. 15 November 2001. Vol. 90, no. 10, p. 5048–5051. [Accessed 1 April 2020]. DOI 10.1063/1.1409582. Available from: http://aip.scitation.org/doi/10.1063/1.1409582
29. WU, Zhongbin, YU, Ling, ZHOU, Xiaokang, GUO, Qingxun, LUO, Jiajia, QIAO, Xianfeng, YANG, Dezhi, CHEN, Jiangshan, YANG, Chuluo and MA, Dongge, 2016ac. Management of Singlet and Triplet Excitons: A Universal Approach to High-Efficiency All Fluorescent WOLEDs with Reduced Efficiency Roll-Off Using a Conventional Fluorescent Emitter. *Advanced Optical Materials* [online]. 1 July 2016. Vol. 4, no. 7, p. 1067–1074. [Accessed 1 April 2020]. DOI 10.1002/adom.201600117. Available from: http://doi.wiley.com/10.1002/adom.201600117
30. MONKMAN, A P, HÜMMELGEN, I A and NASSAR, E J, 2001ad. Singlet Generation from Triplet Excitons in Fluorescent Organic Light-Emitting Diodes. *ISRN Materials Science* [online]. 2001. Vol. 2013. [Accessed 1 April 2020]. DOI 10.1155/2013/670130. Available from: http://dx.
31. ZHELUDEV, Nikolay, 2007ae. *The life and times of the LED - A 100-year history*. April 2007. Nature Publishing Group.
32. TANG, C. W. and VANSLYKE, S. A., 1987af. Organic electroluminescent diodes. *Applied Physics Letters* [online]. 21 September 1987. Vol. 51, no. 12, p. 913–915. [Accessed 3 April 2020]. DOI 10.1063/1.98799. Available from: http://aip.scitation.org/doi/10.1063/1.98799
33. GASPAR, Daniel J. and POLIKARPOV, Evgueni, 2015ag. *OLED fundamentals: Materials, devices, and processing of organic light-emitting diodes*. ISBN 9781466515192.
34. HOU, Liudong, DUAN, Lian, QIAO, Juan, ZHANG, Deqiang, DONG, Guifang, WANG, Liduo and QIU, Yong, 2010ah. Efficient solution-processed small-molecule single emitting layer electrophosphorescent white light-emitting diodes. *Organic Electronics*. 1 August 2010. Vol. 11, no. 8, p. 1344–1350. DOI 10.1016/j.orgel.2010.05.015.
35. Professor Robert B. Laughlin, Department of Physics, Stanford University, [no date]. [online]. [Accessed 4 April 2020 ai]. Available from: http://large.stanford.edu/courses/2007/ph210/hellstrom1/
36. HUNG, L. S., TANG, C. W. and MASON, M. G., 1997aj. Enhanced electron injection in organic electroluminescence devices using an Al/LiF electrode. *Applied Physics Letters* [online]. 13

January 1997. Vol. 70, no. 2, p. 152–154. [Accessed 4 April 2020]. DOI 10.1063/1.118344. Available from: http://aip.scitation.org/doi/10.1063/1.118344

37. COMMISSION INTERNATIONALE DE L'ECLAIRAGE, 2016ak. *The Use of Terms and Units in Photometry-Implementation of the CIE System for Mesopic Photometry* [online]. [Accessed 5 April 2020]. Available from: http://files.cie.co.at/841_CIE_TN_004-2016.pdf
38. DE SA PEREIRA, Daniel;, DATA, Przemyslaw; and MONKMAN, Andrew P., 2017al. Methods of Analysis of Organic Light Emitting Diodes. *Display and Imaging*. 2017. Vol. 2, no. May, p. 323–337.
39. CHOUDHURY, Asim Kumar Roy, [no date]. *Principles of colour and appearance measurement. Volume 2, Visual measurement of colour, colour comparison and management*. ISBN 1782423672.
40. GREINER, Horst, 2007an. Light extraction from organic light emitting diode substrates: Simulation and experiment. *Japanese Journal of Applied Physics, Part 1: Regular Papers and Short Notes and Review Papers*. 2007. DOI 10.1143/JJAP.46.4125.
41. LU, M. H. and STURM, J. C., 2002ao. Optimization of external coupling and light emission in organic light-emitting devices: Modeling and experiment. *Journal of Applied Physics*. 2002. DOI 10.1063/1.1425448.
42. WU, Tien Lin, HUANG, Min Jie, LIN, Chih Chun, HUANG, Pei Yun, CHOU, Tsu Yu, CHEN-CHENG, Ren Wu, LIN, Hao Wu, LIU, Rai Shung and CHENG, Chien Hong, 2018ap. Diboron compound-based organic light-emitting diodes with high efficiency and reduced efficiency roll-off. *Nature Photonics*. 1 March 2018. Vol. 12, no. 4, p. 235–240. DOI 10.1038/s41566-018-0112-9.
43. LIN, Ting-An, CHATTERJEE, Tanmay, TSAI, Wei-Lung, LEE, Wei-Kai, WU, Meng-Jung, JIAO, Min, PAN, Kuan-Chung, YI, Chih-Lung, CHUNG, Chin-Lung, WONG, Ken-Tsung and WU, Chung-Chih, 2016aq. Sky-Blue Organic Light Emitting Diode with 37% External Quantum Efficiency Using Thermally Activated Delayed Fluorescence from Spiroacridine-Triazine Hybrid. *Advanced Materials* [online]. August 2016. Vol. 28, no. 32, p. 6976–6983. [Accessed 6 April 2020]. DOI 10.1002/adma.201601675. Available from: http://doi.wiley.com/10.1002/adma.201601675
44. TSAI, Kuen-Wei, HUNG, Miao-Ken, MAO, Yi-Hen and CHEN, Show-An, 2019ar. Solution-Processed Thermally Activated Delayed Fluorescent OLED with High EQE as 31% Using High Triplet Energy Crosslinkable Hole Transport Materials. *Advanced Functional Materials* [online]. 18 April 2019. Vol. 29, no. 15, p. 1901025. [Accessed 6 April 2020]. DOI 10.1002/adfm.201901025. Available from: https://onlinelibrary.wiley.com/doi/abs/10.1002/adfm.201901025
45. SONG, Jinouk, KIM, Kwon-Hyeon, KIM, Eunhye, MOON, Chang-Ki, KIM, Yun-Hi, KIM, Jang-Joo and YOO, Seunghyup, 2018as. Lensfree OLEDs with over 50% external quantum efficiency via external scattering and horizontally oriented emitters. *Nature Communications* [online]. 10 December 2018. Vol. 9, no. 1, p. 3207. [Accessed 6 April 2020]. DOI 10.1038/s41467-018-05671-x. Available from: http://www.nature.com/articles/s41467-018-05671-x
46. SMITH, T and GUILD, J, 1931at. The C.I.E. colorimetric standards and their use. *Transactions of the Optical Society* [online]. 1931. Vol. 33, no. 3, p. 73. [Accessed 8 April 2020].

DOI 10.1088/1475-4878/33/3/301. Available from: https://iopscience.iop.org/article/10.1088/1475-4878/33/3/301

47. KALYANI, N. Thejo, SWART, Hendrik and DHOBLE, S. J., [no date]. *Principles and applications of organic light emitting diodes (OLEDs)*. ISBN 0081012136.
48. LIU, Baiquan, NIE, Han, ZHOU, Xingbang, HU, Shiben, LUO, Dongxiang, GAO, Dongyu, ZOU, Jianhua, XU, Miao, WANG, Lei, ZHAO, Zujin, QIN, Anjun, PENG, Junbiao, NING, Honglong, CAO, Yong and TANG, Ben Zhong, 2016av. Manipulation of Charge and Exciton Distribution Based on Blue Aggregation-Induced Emission Fluorophors: A Novel Concept to Achieve High-Performance Hybrid White Organic Light-Emitting Diodes. *Advanced Functional Materials* [online]. 2 February 2016. Vol. 26, no. 5, p. 776–783. [Accessed 13 May 2020]. DOI 10.1002/adfm.201503368. Available from: http://doi.wiley.com/10.1002/adfm.201503368
49. MIAO, Yanqin, WANG, Kexiang, ZHAO, Bo, GAO, Long, TAO, Peng, LIU, Xuguang, HAO, Yuying, WANG, Hua, XU, Bingshe and ZHU, Furong, 2018aw. High-efficiency/CRI/color stability warm white organic light-emitting diodes by incorporating ultrathin phosphorescence layers in a blue fluorescence layer. *Nanophotonics* [online]. 1 January 2018. Vol. 7, no. 1, p. 295–304. [Accessed 4 May 2020]. DOI 10.1515/nanoph-2017-0021. Available from: https://www.degruyter.com/view/journals/nanoph/7/1/article-p295.xml
50. REINEKE, Sebastian, LINDNER, Frank, SCHWARTZ, Gregor, SEIDLER, Nico, WALZER, Karsten, LÜSSEM, Björn and LEO, Karl, 2009ax. White organic light-emitting diodes with fluorescent tube efficiency. *Nature* [online]. 14 May 2009. Vol. 459, no. 7244, p. 234–238. [Accessed 4 May 2020]. DOI 10.1038/nature08003. Available from: http://www.nature.com/articles/nature08003
51. HO, Cheuk-Lam, WONG, Wai-Yeung, WANG, Qi, MA, Dongge, WANG, Lixiang and LIN, Zhenyang, 2008ay. A Multifunctional Iridium-Carbazolyl Orange Phosphor for High-Performance Two-Element WOLED Exploiting Exciton-Managed Fluorescence/Phosphorescence. *Advanced Functional Materials* [online]. 25 March 2008. Vol. 18, no. 6, p. 928–937. [Accessed 4 May 2020]. DOI 10.1002/adfm.200701115. Available from: http://doi.wiley.com/10.1002/adfm.200701115
52. LO, Dain, CHANG, Chih Hao, KRUCAITE, Gintare, VOLYNIUK, Dmytro, GRAZULEVICIUS, Juozas V. and GRIGALEVICIUS, Saulius, 2017az. Sky-blue aggregation-induced emission molecules for non-doped organic light-emitting diodes. *Journal of Materials Chemistry C*. 22 June 2017. Vol. 5, no. 24, p. 6054–6060. DOI 10.1039/c7tc01659j.
53. ZHANG, Dongdong, CAI, Minghan, ZHANG, Yunge, ZHANG, Deqiang and DUAN, Lian, 2015ba. Highly Efficient Simplified Single-Emitting-Layer Hybrid WOLEDs with Low Roll-off and Good Color Stability through Enhanced Förster Energy Transfer. *ACS Applied Materials and Interfaces*. 30 December 2015. Vol. 7, no. 51, p. 28693–28700. DOI 10.1021/acsami.5b10783.
54. WANG, Shumeng, ZHAO, Lei, ZHANG, Baohua, DING, Junqiao, XIE, Zhiyuan, WANG, Lixiang and WONG, Wai-Yeung, 2018bb. High-Energy-Level Blue Phosphor for Solution-Processed White Organic Light-Emitting Diodes with Efficiency Comparable to Fluorescent Tubes. *iScience* [online]. 31 August 2018. Vol. 6, p. 128–137. [Accessed 4 May 2020]. DOI 10.1016/j.isci.2018.07.016. Available from: https://linkinghub.elsevier.com/retrieve/pii/S2589004218301044
55. AIZAWA, Naoya, PU, Yong-Jin, WATANABE, Michitake, CHIBA, Takayuki, IDETA, Kazushige, TOYOTA, Naoki, IGARASHI, Masahiro, SUZURI, Yoshiyuki, SASABE, Hisahiro

and KIDO, Junji, 2014bc. Solution-processed multilayer small-molecule light-emitting devices with high-efficiency white-light emission. *Nature Communications* [online]. 18 December 2014. Vol. 5, no. 1, p. 5756. [Accessed 4 May 2020]. DOI 10.1038/ncomms6756. Available from: www.nature.com/naturecommunications

56. ARSENYAN, Pavel, PETRENKO, Alla, LEITONAS, Karolis, VOLYNIUK, Dmytro, SIMOKAITIENE, Jurate, KLINAVIČIUS, Tomas, SKUODIS, Eigirdas, LEE, Jiun-Haw and GRAŽULEVIČIUS, Juozas Vidas, 2019bd. Synthesis and Performance in OLEDs of Selenium-Containing Phosphorescent Emitters with Red Emission Color Deeper Than the Corresponding NTSC Standard. *Inorganic Chemistry* [online]. 5 August 2019. Vol. 58, no. 15, p. 10174–10183. DOI 10.1021/acs.inorgchem.9b01283. Available from: https://pubs.acs.org/doi/10.1021/acs.inorgchem.9b01283
57. THIYAGARAJAN, Manojkumar Dhanthala, BALIJAPALLI, Umamahesh, LEITONAS, Karolis, VOLYNIUK, Dmytro, SIMOKAITIENE, Jurate, KERUCKAS, Jonas, JATAUTIENĖ, Eglė, PATHAK, Madhvesh, IYER, Sathiyanarayanan Kulathu and GRAŽULEVIČIUS, Juozas Vidas, 2020be. Human-eyes-friendly white electroluminescence from solution-processable hybrid OLEDs exploiting new iridium (III) complex containing benzoimidazophenanthridine ligand. *Dyes and Pigments* [online]. March 2020. Vol. 174, no. November 2019, p. 108068. DOI 10.1016/j.dyepig.2019.108068. Available from: https://linkinghub.elsevier.com/retrieve/pii/S0143720819323204
58. KAJI, Hironori, SUZUKI, Hajime, FUKUSHIMA, Tatsuya, SHIZU, Katsuyuki, SUZUKI, Katsuaki, KUBO, Shosei, KOMINO, Takeshi, OIWA, Hajime, SUZUKI, Furitsu, WAKAMIYA, Atsushi, MURATA, Yasujiro and ADACHI, Chihaya, 2015bf. Purely organic electroluminescent material realizing 100% conversion from electricity to light. *Nature Communications* [online]. 19 December 2015. Vol. 6, no. 1, p. 8476. [Accessed 15 April 2020]. DOI 10.1038/ncomms9476. Available from: http://www.nature.com/articles/ncomms9476
59. DACT-II – p-OLED, [no date]. [online]. [Accessed 21 April 2020 bg]. Available from: https://www.p-oled.cn/en/product/dact-ii/
60. SKUODIS, Eigirdas, BEZVIKONNYI, Oleksandr, TOMKEVICIENE, Ausra, VOLYNIUK, Dmytro, MIMAITE, Viktorija, LAZAUSKAS, Algirdas, BUCINSKAS, Audrius, KERUCKIENE, Rasa, SINI, Gjergji and GRAZULEVICIUS, Juozas Vidas, 2018bh. Aggregation, thermal annealing, and hosting effects on performances of an acridan-based TADF emitter. *Organic Electronics* [online]. 1 December 2018. Vol. 63, p. 29–40. [Accessed 17 April 2020]. DOI 10.1016/j.orgel.2018.09.002. Available from: https://linkinghub.elsevier.com/retrieve/pii/S1566119918304610
61. NPD (NPB) | N,N′-Di-[(1-naphthyl)-N,N′-diphenyl]-1,1′-biphenyl)-4,4′-diamine sublimed grade, 99% | Sigma-Aldrich, [no date]. [online]. [Accessed 21 April 2020 bi]. Available from: https://www.sigmaaldrich.com/catalog/product/aldrich/556696?lang=en&region=LT
62. TCTA - Tris(4-carbazoyl-9-ylphenyl)amine 97% | Sigma-Aldrich, [no date]. [online]. [Accessed 21 April 2020 bj]. Available from: https://www.sigmaaldrich.com/catalog/product/aldrich/688053?lang=en&region=LT
63. mCP - 1,3-Bis(N-carbazolyl)benzene 97% | Sigma-Aldrich, [no date]. [online]. [Accessed 21 April 2020 bk]. Available from: https://www.sigmaaldrich.com/catalog/product/aldrich/701874?lang=en&region=LT

64. TSPO1 | Sigma-Aldrich, [no date]. [online]. [Accessed 21 April 2020 bl]. Available from: https://www.sigmaaldrich.com/catalog/product/aldrich/901444?lang=en&region=LT
65. TPBi powder - 500MG size | Sigma-Aldrich, [no date]. [online]. [Accessed 21 April 2020 bm]. Available from: https://www.sigmaaldrich.com/catalog/product/aldrich/806781?lang=en&region=LT
66. DUVENHAGE, Mart Mari, NTWAEABORWA, Martin, VISSER, Hendrik G., SWARTS, Pieter J., SWARTS, Jannie C. and SWART, Hendrik C., 2015bn. Determination of the optical band gap of Alq3 and its derivatives for the use in two-layer OLEDs. *Optical Materials* [online]. 1 April 2015. Vol. 42, p. 193–198. [Accessed 12 April 2020]. DOI 10.1016/j.optmat.2015.01.008. Available from: https://linkinghub.elsevier.com/retrieve/pii/S0925346715000221
67. THE GLOBAL LIGHTING ASSOCIATION, 2018bo. *Application of CIE 13.3-1995 with Associated CRI-based Colour Rendition Properties* [online]. [Accessed 17 April 2020]. Available from: https://www.globallightingassociation.org/images/files/GLA_publication_-_Application_of_CIE_13.3-1995_with_Associated_CRI-based_Colour_Rendition_Properties_-_December_2018_1.pdf
68. THOMAS, K. R.Justin, VELUSAMY, Marappan, LIN, Jiann T, CHIEN, Chin Hsiung, TAO, Yu Tai, WEN, Yuh S, HU, Ya Hui and CHOU, Pi Tai, 2005bp. Efficient red-emitting cyclometaiated iridium(III) complexes containing lepidine-based ligands. *Inorganic Chemistry* [online]. August 2005. Vol. 44, no. 16, p. 5677–5685. [Accessed 10 April 2020]. DOI 10.1021/ic050385s. Available from: https://pubs.acs.org/doi/10.1021/ic050385s
69. BAE, Hye Jin, CHUNG, Jin, KIM, Hyungjun, PARK, Jihyun, LEE, Kang Mun, KOH, Tae Wook, LEE, Yoon Sup, YOO, Seunghyup, DO, Youngkyu and LEE, Min Hyung, 2014bq. Deep red phosphorescence of cyclometalated iridium complexes by o-carborane substitution. *Inorganic Chemistry* [online]. 6 January 2014. Vol. 53, no. 1, p. 128–138. [Accessed 10 April 2020]. DOI 10.1021/ic401755m. Available from: https://pubs.acs.org/doi/10.1021/ic401755m
70. BREDAS, Jean Luc, 2014br. Mind the gap! *Materials Horizons* [online]. 1 January 2014. Vol. 1, no. 1, p. 17–19. [Accessed 12 April 2020]. DOI 10.1039/c3mh00098b. Available from: http://xlink.rsc.org/?DOI=C3MH00098B
71. JUNG, Byung Jun, YOON, Chong Bok, SHIM, Hong Ku, DO, Lee Mi and ZYUNG, Taehyoung, 2001bs. Pure-red dye for organic electroluminescent devices: Bis-condensed DCM derivatives. *Advanced Funtional Materials* [online]. 1 December 2001. Vol. 11, no. 6, p. 430–434. [Accessed 13 April 2020]. DOI 10.1002/1616-3028(200112)11:6<430::AID-ADFM430>3.0.CO;2-G. Available from: http://doi.wiley.com/10.1002/1616-3028%28200112%2911%3A6%3C430%3A%3AAID-ADFM430%3E3.0.CO%3B2-G
72. SU, Ying Ju, HUANG, Heh Lung, LI, Chien Le, CHIEN, Chin Hsiung, TAO, Yu Tai, CHOU, Pi Tai, DATTA, Swarup and LIU, Rai Shung, 2003bt. Highly efficient red electrophosphorescent devices based on iridium isoquinoline complexes: Remarkable external quantum efficiency over a wide range of current. *Advanced Materials* [online]. 5 June 2003. Vol. 15, no. 11, p. 884–888. [Accessed 13 April 2020]. DOI 10.1002/adma.200304630. Available from: http://doi.wiley.com/10.1002/adma.200304630
73. ZHAO, Fangchao, WEI, Ying, XU, Hui, CHEN, Dustin, AHAMAD, Tansir, ALSHEHRI, Saad, PEI, Qibing and MA, Dongge, 2017bu. Spatial exciton allocation strategy with reduced energy loss for high-efficiency fluorescent/phosphorescent hybrid white organic light-emitting diodes. *Materials Horizons*. 1 July 2017. Vol. 4, no. 4, p. 641–648. DOI 10.1039/c7mh00131b.

74. KHADEMI, S., SONG, J. Y., WYATT, P. B., KREOUZIS, T. and GILLIN, W. P., 2012bv. Ambipolar Charge Transport in “Traditional” Organic Hole Transport Layers. *Advanced Materials* [online]. 2 May 2012. Vol. 24, no. 17, p. 2278–2283. [Accessed 14 April 2020]. DOI 10.1002/adma.201103830. Available from: http://doi.wiley.com/10.1002/adma.201103830
75. LIU, Jian, 2017bw. Deep-blue efficient OLED based on NPB with little efficiency roll-off under high current density. *Applied Physics A: Materials Science and Processing*. 1 March 2017. Vol. 123, no. 3, p. 1–6. DOI 10.1007/s00339-017-0840-6.

Scientific achievements of student

List of publications

1. PETRENKO, Alla; **LEITONAS, Karolis**; VOLYNIUK, Dmytro; BARYSHNIKOV, Gleb V.; BELYAKOV, Sergey; MINAEV, Boris F.; ÅGREN, Hans; DURGARYAN, Ranush; GRAŽULEVIČIUS, Juozas Vidas; ARSENYAN, Pavel. Benzoselenophenylpyridine platinum complexes: green versus red phosphorescence towards hybrid OLEDs. *Dalton Transactions*. Cambridge: Royal Society of Chemistry, 2020, vol. 49, iss. 11, pp. 3393-3397. ISSN 1477-9226. eISSN 1477-9234. doi: 10.1039/d0dt00214c
2. THIYAGARAJAN, Manojkumar Dhanthala; BALIJAPALLI, Umamahesh; **LEITONAS, Karolis**; VOLYNIUK, Dmytro; SIMOKAITIENE, Jurate; KERUCKAS, Jonas; JATAUTIENE, Egle; PATHAK, Madhvesh; IYER, Sathiyanarayanan Kulathu; GRAŽULEVIČIUS, Juozas Vidas. Human-eyes-friendly white electroluminescence from solution-processable hybrid OLEDs exploiting new iridium (III) complex containing benzoimidazophenanthridine ligand. *Dyes and Pigments*. Oxford: Elsevier, 2020, vol. 174, art. no. 108068, pp. 1-8. ISSN 0143-7208. eISSN 1873-3743. doi: 10.1016/j.dyepig.2019.108068
3. ARSENYAN, Pavel; PETRENKO, Alla; **LEITONAS, Karolis**; VOLYNIUK, Dmytro; SIMOKAITIENE, Jurate; KLINAVIČIUS, Tomas; SKUODIS, Eigirdas; LEE, Jiun-Haw; GRAŽULEVIČIUS, Juozas Vidas. Synthesis and performance in OLEDs of selenium-containing phosphorescent emitters with red emission color deeper than the corresponding NTSC standard. *Inorganic chemistry*. Washington, DC: ACS publications, 2019, vol. 58, iss. 15, pp. 10174-10183. ISSN 0020-1669. eISSN 1520-510X. doi: 10.1021/acs.inorgchem.9b01283
4. VIGANTE, Brigita; **LEITONAS, Karolis**; VOLYNIUK, Dmytro; ANDRULEVICIENE, Viktorija; SIMOKAITIENE, Jurate; IVANOVA, Anna; BUCINSKAS, Audrius; GRAZULEVICIUS, Juozas Vidas; ARSENYAN, Pavel. Synthesis of linear and V-shaped carbazolyl-substituted pyridine-3,5-dicarbonitriles exhibiting efficient bipolar charge transport and E-type fluorescence. *Chemistry - A European journal*. Weinheim: Wiley-VCH, 2019, vol. 25, iss. 13, pp. 3325-3336. ISSN 0947-6539. eISSN 1521-3765. doi: 10.1002/chem.201805323
5. ELTAN, Tugce; LAPIENYTĖ, Liveta; KERUCKIENĖ, Rasa; **LEITONAS, Karolis**; SIMOKAITIENĖ, Jūratė; BUIKA, Gintaras; GRAŽULEVIČIUS, Juozas Vidas. Electroactive D-A derivatives bearing 2,3-dimethylindole and tetrafluorostyrene moieties: synthesis, polymerization, DFT calculations and photophysical properties. *Molecular crystals and liquid crystals*. Oxon: Taylor & Francis, 2018, vol. 671, iss. 1, pp. 24-32. ISSN 1542-1406. eISSN 1563-5287. doi: 10.1080/15421406.2018.1542082

Conferences

1. **LEITONAS, Karolis**; TOMKEVIČIENĖ, Aušra; GRAŽULEVIČIUS, Juozas Vidas. Metal-free room temperature phosphorescent organic materials: poster. In: *Open readings 2019: 62nd international conference for students of physics and natural sciences, March 19-22, Vilnius, Lithuania: abstract book.* Vilnius: Vilnius University, 2019, P1-90, pp. 168-168. ISBN 9786090701379
2. **LEITONAS, Karolis**; KERUCKIENE, Rasa; VOLYNIUK, Dmytro; GRAZULEVICIUS, Juozas Vidas. Organic Room-Temperature Phosphorescence of Phenothiazine and Benzotrifluoride Derivatives for Optical Oxygen Sensors. In: *"π-EJ 2019*". Zabrze. 2019.

3. **LEITONAS, Karolis**; KERUCKIENE, Rasa; VOLYNIUK, Dmytro; GRAZULEVICIUS, Juozas Vidas. Investigation of room-temperature phosphorescence sensitivity to oxygen using benzotrifluoride and phenothiazine derivatives. In: *Open Readings 2020: 63rd international conference for students of physics and natural sciences, March 17-20, Vilnius, Lithuania: abstract book*. Vilnius: Vilnius University, 2020, P3-5, pp. 333-333. ISBN 9786090703779